Sidewall cell envelope synthesis and remodeling in pole-growing mycobacteria

Alam García-Heredia[a], Amol Arunrao Pohane[b], Emily S. Melzer[b], Taylor J. Fiolek[c], Sarah R. Rundell[c], Hoong Chuin Lim[d], Jeffrey Wagner[e], Yasu S. Morita[a,b], Benjamin M. Swarts[c], M. Sloan Siegrist[a,b,#]

[a]Molecular and Cellular Biology Graduate Program, University of Massachusetts, Amherst, Massachusetts, USA; [b]Department of Microbiology, University of Massachusetts, Amherst, Massachusetts, USA; [c]Department of Chemistry and Biochemistry, Central Michigan University, Mount Pleasant, Michigan, USA; [d]Department of Microbiology and Immunobiology, Harvard Medical School, Boston, Massachusetts USA; [e]Department of Immunology and Infectious Disease, Harvard T.H. Chan School of Public Health, Boston, Massachusetts, USA

Running title: Cell envelope assembly along the mycobacterial sidewall

[#]Address correspondence to M. Sloan Siegrist, siegrist@umass.edu

A.G.-H. and A.P. contributed equally to this article.

Abstract

Mycobacteria are rod-shaped cells that expand from their tips. This mode of elongation is distinct from that of well-characterized bacilli and poses unique theoretical challenges to cell envelope homeostasis. Specifically, if polar growth and septation are the only mechanisms by which mycobacteria alter envelope chemistry, it is unclear if and how these organisms actively maintain the integrity of their lateral cell surface. Previous studies have shown both polar and sidewall localization of enzymes that catalyze envelope precursor synthesis and of proteins that polymerize and crosslink peptidoglycan. Since envelope synthesis around the cell periphery could provide a means by which to edit and protect this critical, multi-layered barrier, we sought to test whether these enzymes are active outside of elongation and division sites. Labeling experiments with peptidoglycan and mycomembrane probes revealed that envelope deposition or modification occur in uneven polar gradients that continue along the sidewall. All of the peptidoglycan probes tested were sensitive to L,D-transpeptidase activity, including D-alanine-D-alanine derivatives that we show incorporate into cytoplasmic precursors of the biopolymer. Lateral labeling by the dipeptide probe persisted when periplasmic remodeling was inhibited, suggesting that peptidoglycan metabolism in these regions includes precursor synthesis. Mycobacterial cell expansion, however, was restricted to the poles. Our observations suggest a post-expansion role for envelope assembly along the sidewall and provide a conceptual framework for understanding cell-wide envelope robustness in the face of polar growth.

Introduction

Model, rod-shaped organisms such as *Escherichia coli* and *Bacillus subtilis* elongate across a broad swath of the cell (1, 2). By contrast, mycobacterial cells extend from narrow, polar or subpolar regions (3-9). Circumscription of growth to discrete zones poses spatial challenges to the bacterial cell. For example, elongation and division in *E. coli* are coordinated via interactions between the complexes that mediate these processes (10, 11). It is unclear how or whether similar contacts occur in mycobacteria if the elongasome at the cell tip is sequestered from the divisome at the cell center. Furthermore, the cell poles of species that expand along the sidewall are thought to be inert. If polar (or subpolar) growth and division are the only sites of peptidoglycan synthesis in mycobacteria, the entire lateral surface of the cell must be inert (3, 12-14). Such an expanse of non-renewable surface could leave the cell vulnerable to environmental insults, impair its ability to take up nutrients, or compromise its ability to maintain its shape.

The mycobacterial cell envelope is comprised of the covalently-bound biopolymers peptidoglycan, arabinogalactan and mycolic acids, as well as intercalated glycolipids and a thick capsule (15). While fluorescent protein fusions to enzymes that catalyze the terminal cytosolic steps of mycobacterial envelope synthesis localize strongly to growth poles, they also decorate the sidewall (5, 16, 17). The transporter for mycolic acid precursors is likewise enriched at mycobacterial cell tips but present along lateral surfaces (18). Close inspection of images of the periplasmic penicillin-binding proteins that stitch together the peptidoglycan polymer reveals that they, too, may have weak affinity for the sidewall in addition to their primary polar perch (9, 19-21). Since expansion of the mycobacterial cell has only been demonstrated at its tips, one interpretation of these data is that the sidewall-localized enzymes and transporter are artifacts of tagging or that they are inactive (22, 23). Alternatively, these enzymes may be active but not

part of complexes at the ends and middle of the cell. Such an arrangement may facilitate an efficient transition between elongation and division. It may also allow the organism to edit what might otherwise be an expanse of inert envelope.

One strategy for tracking envelope constituents is metabolic labeling of the bacterial cell surface (24). An envelope precursor or 'probe' bearing a reactive group is incorporated into the envelope by the endogenous enzymatic machinery of the cell. The presence of the probe is then revealed by a chemical reaction with an exogenous label that bears a complementary reactive group. It is now possible to mark peptidoglycan in a wide range of bacteria (1, 13, 25-28) as well as the lipopolysaccharide in the Gram-negative outer membrane (29, 30) and various mycobacteria-specific glycoconjugates (31-34). In some cases the probe can be pre-labeled, bypassing the chemical ligation step and embedding the detection moiety directly into the macromolecule (13, 24, 28, 31, 35-37).

Optimized labeling by envelope probes does not inhibit bacterial growth and can be used to extract precise spatial information within minutes of incubation (24). In theory, this technique is well-suited for asking when and where envelope synthesis occurs and, therefore, for testing whether sidewall-localized synthetic enzymes are active in pole-growing mycobacteria. Indeed D-amino acid probes, which in other species have been shown to incorporate into peptidoglycan (1, 13, 25), label both the poles and sidewall of mycobacteria (22, 25, 38-40) even with incubation times well under one generation. However, both intracellular and extracellular incorporation pathways have been characterized or hypothesized for these reagents, complicating the interpretation of labeling patterns (24). Intracellular uptake implies that the probe enters the biosynthetic pathway at an early stage, and therefore marks nascent envelope. Extracellular incorporation, on the other hand, suggests that the probe enters the pathway at a later stage and/or is part of enzymatic remodeling of the macromolecule in question. The extent

to which envelope synthesis and remodeling are linked is not clear (12, 13, 25, 41-43) and may vary with species and external milieu. In *Mycobacterium tuberculosis*, for example, there is indirect but abundant data that suggest that there is substantial envelope remodeling during infection when growth and envelope synthesis are presumed to be slow or nonexistent (7).

An intracellular metabolic tagging method for peptidoglycan would be an ideal tool for determining whether tip-extending mycobacteria can synthesize envelope along the lateral surface of the cell. At least two pieces of evidence suggest that D-alanine-D-alanine dipeptide probes may be incorporated into peptidoglycan via the cytoplasmic MurF ligase (27, 44). First, alkynyl derivatives of D-alanine-D-alanine rescue the growth of *Chlamydia trachomatis* treated with D-cycloserine, an antibiotic that inhibits peptidoglycan synthesis by inhibiting the production and self-ligation of D-alanine in the cytoplasm (27). Second, *B. subtilis* cells stripped of mature peptidoglycan by lysozyme treatment retain a small amount of dipeptide-derived fluorescence (44). While these data are suggestive, formal demonstration of intracellular incorporation requires direct evidence that the probe labels peptidoglycan precursors. Given that the muropeptide is also a substrate for trans-, carboxy- and endopeptidases, an additional, outstanding question in the field is how labeling by amino acid-based derivatives is impacted by periplasmic remodeling. More broadly, better characterization of the metabolic fate of probes can increase user confidence in and precision of conclusions that can be drawn from labeling experiments (45, 46).

We sought to test whether peptidoglycan synthesis in mycobacteria is restricted to sites of cell expansion. All of the D-amino acid probes in our panel labeled the poles and sidewalls of *M. smegmatis* and *M. tuberculosis* cells, as did probes specific for components of the mycomembrane. Consistent with what has been reported previously, however, we do not detect obvious surface expansion along the periphery of the cell. Monopeptide D-amino acid probes

accessed multiple uptake pathways but chiefly reported peptidoglycan remodeling by L,D-transpeptidases. Dipeptide probes complemented defects in D-alanine synthesis or ligation and were present in lipid-linked peptidoglycan precursors, suggesting that they mark synthesis of the biopolymer. Although dipeptide labeling was unexpectedly sensitive to the presence of L,D-transpeptidases, sidewall signal was preserved upon inhibition of periplasmic remodeling. Our data suggest that the periphery of the mycobacterial cell is not an inert surface, but rather that it is a region of active envelope synthesis and remodeling. Such activity does not directly support division or elongation but may allow editing of a complex, essential structure at timescales faster than those permitted by zonal growth.

Results

Penicillin-binding proteins localize to the poles and sidewall. Peptidoglycan synthesis is a highly conserved process. The final, lipid-linked precursor lipid II is synthesized by MurG on the cytoplasmic side of the plasma membrane then flipped to the periplasm, where it is incorporated into the existing meshwork (47). Our previous work with GFP and monomeric RFP (mRFP) and mCherry fusions to MurG and to the terminal, cytoplasmic enzymes for arabinogalactan and mycomembrane precursor synthesis suggested that the proteins colocalize near sites of polar growth and additionally form weaker, uncoordinated foci along the lateral surface (5, 16, 17).

The presence of MurG along the periphery of the mycobacterial cell could suggest that the peptidoglycan precursors are synthesized in these locations. In other species, transglycosylases from both the PBP (penicillin-binding proteins) and SEDS (shape, elongation, division, and sporulation) families stitch MurG-derived subunits into existing peptidoglycan (47-50). If MurG contributes to peptidoglycan synthesis along the lateral surface of the mycobacterial cell, at least a subset of these periplasmic enzymes must be present at the sidewall to assemble the

biopolymer. Two conserved PBPs in mycobacteria are likely responsible for most of the peptidoglycan polymerization required for cell viability, PonA1 and PonA2 (7, 20, 51). Published images of PonA1-mRFP and PonA1-mCherry localization suggested that the fusion proteins might decorate the mycobacterial sidewall in addition to the cell tips (9, 19, 20), but the resolution of the PonA1-mRFP micrographs did not allow for definitive assignment. Therefore, we first verified the localization of this fusion protein. We found that a subset of protein indeed homes to the lateral cell surface (**Fig. S1A**).

We were concerned that expression of PonA1-mRFP causes aberrant polar morphology and is toxic to *M. smegmatis* (19, 20) and about the propensity of mCherry to cluster (52). Since our attempts to produce PonA1 fusions with different fluorescent proteins were unsuccessful, we opted to take a complementary, activity-based approach. Fluorescent derivatives of β-lactam antibiotics bind specifically and covalently to PBPs, and therefore have been used to image active enzyme in both protein gels and intact cells (53). Our images of whole cells labeled with Bocillin, a BODIPY conjugate of penicillin, were in agreement with those from a previous publication (21), and seemed to indicate that Bocillin binds both the poles and sidewall of *M. smegmatis* (**Figs. S1B, S1C**). However, given the hydrophobicity of the BODIPY dye, we considered the possibility that Bocillin might nonspecifically associate with the greasy mycomembrane. Fluorescence across the cell surface was diminished by pre-treating cells with the β-lactam ampicillin, which prevents peptidoglycan assembly by binding to PBPs, but not D-cycloserine, which inhibits peptidoglycan synthesis in a PBP-independent manner (**Figs. S1B, S1C**). These data suggest that at least some of the sidewall labeling of Bocillin is specific, and therefore, that PBPs are present in these locations.

Metabolic labeling of mycobacterial envelope comprises asymmetric polar gradients. The presence of MurG and PBPs is necessary but not sufficient for peptidoglycan synthesis. It is

possible, for example, that these enzymes lack the necessary building blocks to make and/or polymerize precursors. Therefore we sought to visualize this process by directly marking nascent biopolymer. Fluorescent vancomycin, which binds uncrosslinked peptidoglycan pentapeptides, revealed both polar and lateral patches (**Fig. S2**) as previously noted (8). Since labeling is not exclusive to newly synthesized biopolymer, we sought a complementary strategy for marking new peptidoglycan. We and others have shown that D-amino acid derivatives incorporate into peptidoglycan and can be used for labeling a diverse array of species *in situ* (1, 13, 25, 27, 28, 37), including *M. smegmatis* and *M. tuberculosis* (22, 25, 38, 39). Metabolic labeling can be achieved by a one-step process, in which the fluorophore is directly appended to the amino acid, or a two-step process in which a small chemical tag on the D-amino acid is detected by subsequent reaction with a fluorescent reactive partner (24). We first reexamined the localization patterns of various D-amino acid probes reported in the literature, including RADA (13), which is directly conjugated to 5-carboxytetramethylrhodamine, and the two-step alkyne-D-alanine (alkDA or EDA, (13, 25)), and alkyne-D-alanine-D-alanine (alkDADA or EDA-DA, (54); we use the metabolic labeling nomenclature originally adopted in (55)) which we detected by copper-catalyzed azide-alkyne cycloaddition (CuAAC) after fixation (**Fig. S3**). After the cells were incubated for ~10% generation in probe, high resolution and quantitative microscopy revealed that they had asymmetric, bidirectional gradients of fluorescence that emanated from the poles and continued along the sidewall (**Fig. 1A**). The gradients were also apparent in live cells when we detected azido-D-alanine-D-alanine (azDADA or ADA-DA, (27)) dipeptide incorporation by either CuAAC (using low copper, bio-friendly reaction conditions ((56), **Fig. S4A**) or by copper-free, strain-promoted azide-alkyne cycloaddition (SPAAC, **Fig. S4B**).

Assembly of the three, covalently-bound layers of the mycobacterial envelope—peptidoglycan, arabinogalactan and the mycomembrane—has long been presumed to be spatially coincident.

This is largely based on biochemical data suggesting that ligation of arabinogalactan to peptidoglycan occurs concurrently with crosslinking of the biopolymer by transpeptidases (57). We and others have found that cytoplasmic enzymes that mediate arabinogalactan and mycomembrane synthesis are enriched at the poles but also present along the periphery of the cell (5, 16, 18), as is metabolic labeling by OalkTMM and NalkTMM ((31-33), **Fig. 1A**). OalkTMM and NalkTMM are trehalose monomycolate derivatives that predominantly mark covalent mycolates and trehalose dimycolate, respectively, in the mycomembrane (33). Since the azido and alkynyl groups on the different probes are not orthogonal to eachother, we opted to compare peptidoglycan and mycomembrane labeling patterns by using RADA as a fiducial marker. The cell pole with brighter RADA fluorescence also had more alkDADA or OalkTMM labeling (**Fig. 1B**), suggesting that the polar orientation of peptidoglycan and mycomembrane metabolism is coincident. We then compared the fluorescence intensity profiles of cells that had been individually labeled with the probes, and found similar, average distributions of RADA, alkDADA and OalkTMM at the poles and peripheries of the cells (**Fig. 1C**).

We next sought to address whether the cell envelope of the related *M. tuberculosis* is also labeled in polar gradients. We previously showed that alkDA incorporates into the cell surface of the organism (25) but were unable to stain the entire population of bacteria. To investigate the origin of labeling heterogeneity, we first tested whether the structure of fluorophore (**Fig. S3**) influenced probe incorporation by incubating *M. tuberculosis* in HADA, NADA or RADA and assessing population fluorescence by flow cytometry. HADA and NADA incubation yielded single, well-defined fluorescent populations (**Fig. S5A**). RADA also labeled the entire *M. tuberculosis* population, albeit with greater cell-to-cell variability in fluorescence intensity. Given that *M. tuberculosis* incorporates fluorescent probes HADA and NADA relatively evenly across the population, we hypothesized that the apparent heterogeneity that we previously observed for alkDA labeling (25) was the result of an inefficient CuAAC ligation. We obtained modest

improvements by changing the reaction conditions, more specifically, by swapping the BTTP ligand (56, 58) for TBTA, altering the ratio of ligand:Cu(I) and increasing the azide label concentration. We also switched our detection moiety to an azide appended to hydroxycoumarin, the same small, uncharged fluorophore as the one-step HADA probe (**Fig. S3**). Under our optimized conditions we detected azido-coumarin fluorescence from ~15-20% of cells that had been incubated in alkDA, alkDADA or OalkTMM (**Figs. S5B**).

Although unable to achieve homogenous *M. tuberculosis* labeling with two-step envelope probes, we decided to test whether the sites of envelope labeling in the limited fluorescent subpopulation resemble those of *M. smegmatis*. HADA, alkDADA and OalkTMM tagging all produced cells that had a mixture of sidewall and polar fluorescence (**Fig. S5C**) but exhibited a higher degree of cell-to-cell variability compared to *M. smegmatis* (**Fig. 1A**). Quantitation of HADA fluorescence showed that peptidoglycan transformations comprised asymmetric polar gradients when averaged across the population (**Fig. 1D)**. We next asked whether there was a cell-wide difference in labeling distribution in *M. tuberculosis* compared to *M. smegmatis*. We arbitrarily defined the dimmer polar region as the first 25% of the cell length, the sidewall as the middle 50%, and the brighter polar region as the final 25%. In a cell with perfect, circumferential labeling, the ratio of dim pole:sidewall:fast pole in a cell would be 25:50:25. Since HADA labeled a large proportion of *M. tuberculosis* (**Fig. S5A**) and was more resistant to photobleaching than NADA, we compared these ratios for HADA in septating and non-septating *M. smegmatis* and *M. tuberculosis* labeled for ~10% generation time (**Fig. 1D**). For *M. smegmatis*, the ratios were 15:38:47 for non-septating cells and 17:39:43 for septating cells, while for *M. tuberculosis*, they were 21:47:32 and 17:56:27 for *M. tuberculosis*. These data suggest that a greater proportion of peptidoglycan labeling in *M. tuberculosis* likely occurs along the cell periphery than in *M. smegmatis*, although we cannot rule out a differential contribution of cyan autofluorescence in the two species (59).

Expansion of the mycobacterial envelope is concentrated at the poles. Dispersed elongation is well-characterized in model organisms such as *E. coli* and *B. subtilis* but has not been reported in mycobacteria. We were intrigued by the sidewall metabolic labeling of the *M. smegmatis* and *M. tuberculosis* cell envelope. This was not an artifact of CuAAC since one-step fluorescent probe incubation yielded the same pattern and no probe/CuAAC controls did not. Nor was the sidewall signal an artifact of metabolic labeling, as fluorescent vancomycin staining of uncrosslinked peptidoglycan revealed lateral patches (**Fig. S4**) as previously noted (8). The localization of the probes is also supported by the presence of cell envelope synthesis enzymes that reside on either side of the plasma membrane ((5, 9, 16, 17, 19-21) and **Fig. S1**). We performed a pulse chase experiment to test whether cell expansion correlates with probe-marked sites of envelope synthesis and remodeling. After labeling peptidoglycan with RADA, we briefly tagged surface-exposed primary amines with an NHS ester dye conjugated to AlexaFluor 488 (NHS488) and tracked labeled and unlabeled cell surface during outgrowth. Consistent with previous reports (3-5), time-lapse imaging showed that fluorescence dilution is asymmetric and is restricted to the poles (**Fig. S6**).

Intracellular and extracellular pathways of D-amino acid probe incorporation in mycobacteria. OalkTMM and NalkTMM are inserted directly by the extracellular Antigen 85 complex into the mycomembrane (33). However, there are three potential pathways by which D-amino acid probes might incorporate into mycobacterial peptidoglycan (24, 60, 61): an intracellular, biosynthetic route and two extracellular routes, mediated by D,D-transpeptidase or L,D-transpeptidase remodeling enzymes (**Fig. 2A**). Peptidoglycan remodeling, particularly by the L,D-transpeptidases abundantly encoded in the mycobacterial genome, may not strictly correlate with synthesis of the biopolymer (12, 41, 43). Therefore, we sought to distinguish between the different routes of incorporation for D-amino acid probes in mycobacteria.

It seemed possible that the chemical structure of the derivative (**Fig. S3**) and/or number of labeling steps might influence probe uptake, so we first tested the labeling sensitivity of a panel of envelope probes to antibiotics that inhibit potential incorporation routes (**Fig. 2A**). We also assessed OalkTMM and the D-alanine-D-alanine dipeptide probe, the latter of which has been proposed to tag the peptidoglycan of other species via the cytoplasmic MurF ligase (44, 54). D-cycloserine inhibits the D-alanine racemase (Alr) and ligase (DdlA) in mycobacteria (62). Together with the β-lactamase inhibitor clavulanate, β-lactams like ampicillin block D,D-transpeptidases and D,D-carboxypeptidases. Broader-spectrum derivatives of β-lactams, the carbapenems, additionally inhibit L,D-transpeptidases (63). We also included vancomycin, an antibiotic that interferes with transpeptidation and transglycosylation by steric occlusion, to control for general defects in periplasmic peptidoglycan assembly. Labeling for all single residue D-amino acid probes decreased significantly in response to imipenem or D-cycloserine treatment (**Fig. 2B**). By contrast, labeling by the dipeptide probe was relatively resistant to these antibiotics. Neither vancomycin nor ampicillin had a clear effect on labeling by any of the probes, indicating that inhibition of growth, disruption of peptidoglycan polymerization, and abrogration of D,D-transpeptidation do not explain the metabolic incorporation differences. OalkTMM labeling was sensitive to D-cycloserine, but not to imipenem or ampicillin, suggesting that transfer of mycolates to arabinogalactan may require peptidoglycan precursor synthesis but not transpeptidation.

To test whether distinct mechanisms of probe incorporation were inhibited by D-cycloserine and imipenem, we performed chemical epistasis experiments in which we assessed fluorescent D-amino acid labeling in the presence of each drug alone or in combination. Imipenem and ampicillin did not have additive effects on HADA labeling (**Fig. 2C**). These data are consistent with the notion ampicillin does not significantly impact probe incorporation and/or that the

antibiotics have overlapping targets. D-cycloserine was additive with imipenem, suggesting that the antibiotics block both overlapping and separate pathways of HADA incorporation. Thus the effect of D-cycloserine on D-amino acid labeling appears to be specific and likely stems from both direct inhibition of cytoplasmic incorporation and from depriving L,D-transpeptidases of acceptor muropeptides. Although ampicillin alone did not impact cell fluorescence (**Fig. 2C**), it was also additive with D-cycloserine, suggesting that D,D-transpeptidases may incorporate D-amino acids when cytoplasmic uptake is blocked. In aggregate, these experiments are most consistent with multiple routes of D-amino acid incorporation into mycobacterial peptidoglycan: L,D-transpeptidase and cytoplasmic and, under specific circumstances, D,D-transpeptidase.

RADA and NADA labeling was more sensitive to imipenem than HADA and alkDA (**Figs. 2B**), at multiple concentrations of drug (**Fig. 2D**). To test whether the probes were differentially incorporated by L,D-transpeptidases, we knocked out three of the six enzymes encoded in the *M. smegmatis* genome. We chose to focus on LdtA, LdtB and LdtE since the *M. tuberculosis* homologs (Ldt_{MT1}, Ldt_{MT2}, and Ldt_{MT4}, respectively) have been shown *in vitro* to have both cross-linking and D-amino acid exchange activity and to be inhibited by imipenem (64). RADA and NADA fluorescence decreased by ~80-85% the absence of *ldtABE,* and this effect was complemented by the expression of *ldtA* alone (**Fig. 2E**). We observed a more moderate effect on HADA and alkDA labeling, which were respectively decreased by ~40-60%. Collectively these data suggest that: 1. RADA and NADA probes primarily report L,D-transpeptidase activity, tetrapeptide substrate, or both, and 2. HADA and alkDA likely label via both cytoplasmic and L,D-transpeptidase routes.

Dipeptide D-amino acid probe incorporates into mycobacterial peptidoglycan precursors. Previous reports have suggested that D-alanine-D-alanine dipeptide probes are incorporated into peptidoglycan of other species via an intracellular, MurF-dependent route (**Fig. 2A**, (27,

44)). D-alanine is produced in mycobacteria by Alr, the D-alanine racemase. The molecule is linked to a second D-alanine by DdlA, the D-alanine ligase, and the resulting dipeptide is added to the UDP-MurNAc-tripeptide by MurF. If the alkDADA probe labels mycobacterial peptidoglycan via MurF, addition of the molecule to the growth medium should rescue a mutant that is unable to make D-alanine-D-alanine. We first constructed an *alr* deletion mutant in *M. smegmatis* and verified that growth is rescued by exogenous D-alanine but not by alkDA (**Fig. 3A**). Although our antibiotic data suggest that alkDA is incorporated into peptidoglycan in part via a cytoplasmic pathway (**Figs. 2B, 2E**), the inability of this probe to rescue growth was not surprising given the substrate specificites of Ddl and MurF (65) and inefficient synthesis of UDP-MurNAc-pentapeptide using D-amino acids other than alanine (60). In contrast to the alkDA results, we were able to rescue *alr* with either D-alanine-D-alanine or its alkynyl derivative (**Fig. 3A**).

We considered the possibility that alkDADA may be digested by a D,D-carboxypeptidase prior to incorporation. This would result in the release of both unlabeled D-alanine and alkDA, the first of which could account for *alr* growth rescue (**Fig. 3A**). We reasoned that a more precise gauge for MurF-dependent incorporation of the intact probe would be whether it could support the replication of a strain unable to ligate D-alanine to itself. Therefore, we confirmed that alkDADA rescues the growth of a temperature-sensitive *ddlA* mutant (66) at the non-permissive temperature (**Fig. 3B**).

Our genetic data supported a MurF-dependent pathway of alkDADA incorporation into peptidoglycan. If true, the probe should be present in peptidoglycan precursors such as lipid I and II. To test this hypothesis, we first optimized for mycobacteria a recently-reported protocol for detecting lipid-linked precursors (67, 68). We extracted lipidic species from *M. smegmatis* and exchanged endogenous D-alanines for biotin-D-lysine *in vitro* using purified *Staphylococcus*

aureus enzyme PBP4, a promiscuous D,D-transpeptidase (67-69). Biotinylated species were separated by SDS-PAGE and detected by horseradish peroxidase-conjugated streptavidin. We detected a biotin-linked, low molecular weight band that is reduced upon D-cycloserine treatment and accumulates when the lipid II flippase MurJ (MviN, (70)) is depleted or in the presence of vancomycin (**Fig. 4A**), conditions that have been shown to dramatically enhance precursor detection in other species (67, 68). These data strongly suggest that the BDL-marked species are lipid-linked peptidoglycan precursors. We next turned our attention to detecting lipid I/II from *M. smegmatis* incubated with alkDADA. Initially we were unable to identify alkDADA-labeled species from organic extracts of *M. smegmatis* that had been subjected to CuAAC ligation with picolyl azide biotin (**Fig. 4B**). We reasoned that the proportion of labeled precursors might be below our limit of detection. Accordingly, we repeated the experiment in the *Δalr* background and found that we could clearly detect a low molecular-weight species band that accumulated with vancomycin treatment (**Fig. 4B,** top) and that ran at the same size as BDL-labeled material (**Fig. 4B,** bottom). We were also able to identify a low molecular weight species from *Δalr* incubated with azido-D-alanine-D-alanine (azDADA) that was revealed by either CuAAC or SPAAC ligation to alkyne- or cyclooctyne-biotin, respectively (**Fig. 4C**). Taken together, our genetic and biochemical experiments show that the alkDADA and azDADA dipeptide probes insert into mycobacterial peptidoglycan precursors by a MurF-dependent route.

Sidewall labeling by dipeptide D-amino acid probe persists when periplasmic remodeling is inhibited. We noted previously that alkDADA labeling was relatively stable to imipenem treatment (**Figs. 2B. 2D**). This was consistent with the notion that the probe incorporates via a cytoplasmic, MurF-dependent pathway (**Figs. 3, 4**). However we were surprised to observe that alkDADA labeling decreased in the absence of LdtA, LdtB, LdtE or combinations thereof (**Fig. 5A**).

Although carbapenems have *in vitro* activity against *M. tuberculosis* LdtA, LdtB and LdtE (64), imipenem may block a different subset of the six L,D-transpeptidases encoded in the *M. smegmatis* genome. Accordingly we tested whether the perturbations were epistatic to one another by comparing the effect of antibiotic treatment in wildtype and *ΔldtABE*. We chose to use RADA labeling as our readout as this probe has similar sensitivity to imipenem and *ldt* mutation (**Fig. 2E**). The antibiotic had significantly less effect on labeling in the *ΔldtABE* strain than in wildtype *M. smegmatis* (**Fig. 5B**), suggesting that the two perturbations impact overlapping pathways with respect to RADA incorporation.

The epistasis experiment confirmed that imipenem impinges on LdtA, LdtB and/or LdtE activity in *M. smegmatis*. We next considered the idea that inhibition of another target(s) of imipenem might permit alkDADA labeling even when L,D-transpeptidases are inhibited by the antibiotic. Indeed, carbapenems like imipenem are known to target D,D-carboxypeptidases in *M. tuberculosis* (63) and we likewise find increased fluorescent vancomycin labeling in imipenem-treated *M. smegmatis* (**Fig. S8**). Imipenem as well as ampicillin completely rescued alkDADA labeling in the *ΔldtABE* mutant (**Fig. 5C**). The effect of the antibiotics was specific, since occlusion of transpeptidation by vancomycin did not bolster fluorescence, and not additive, suggesting that they increased labeling via the same mechanism. These data suggest that promiscuous targeting of periplasmic remodeling enzymes by imipenem restores dipeptide probe labeling even when L,D-transpeptidases are inhibited.

Our primary motivation for characterizing D-amino acid probe incorporation was to identify a reagent that would allow us to test directly whether the mycobacterial sidewall is a site of peptidoglycan synthesis. In mycobacteria we find that monopeptide probes are taken up to varying extents by L,D-transpeptidases (**Fig. 2**), making them sub-optimal for this purpose.

Although the dipeptide probes are incorporated into peptidoglycan precursors (**Figs. 4B**, **4C**), fluorescence derived from alkDADA was also sensitive to L,D-transpeptidase activity (**Fig. 5A**). However this unexpected sensitivity could be prevented by inhibiting one or more targets common to imipenem and ampicillin (**Fig. 5C**), suggesting that short-term application of these antibiotics may enhance or restore the specificity of alkDADA labeling for peptidoglycan synthesis. Importantly, we find that alkDADA signal at the poles and along the sidewall is stable to imipenem treatment (**Fig. 5D**). Persistent alkDADA labeling along the cell periphery despite diminished periplasmic remodeling activity suggests that peptidoglycan precursor synthesis occurs in this region.

Discussion

In this work we aimed to address the seemingly discrepant observations that, on the one hand, mycobacteria grow from the cell poles ((3-9), **Fig. S6**), and on the other, that cell envelope synthetic enzymes are enriched at the poles but also present along the sidewall ((5, 9, 16, 19-21), **Fig. S1**). The first step to resolving this conundrum is to unambiguously identify sites of active cell envelope metabolism. Although the D-amino acid probes that we and others have developed for peptidoglycan labeling have been extensively used for this purpose (24), in most cases it has not been clear whether they report the location(s) of cytoplasmic synthesis, periplasmic exchange or a combination of processes.

Here we show that in *M. smegmatis* the metabolic fate of monopeptide probes is partially dependent on the substituent; whereas NBD and TAMRA-conjugated D-amino acids are primarily exchanged into mycobacterial peptidoglycan by L,D-transpeptidases, their alkyne and coumarin-conjugated counterparts appear to incorporate by both extracellular and intracellular pathways (**Fig. 2**). While many publications note that D-amino acid probes are taken up via

periplasmic transpeptidases, our data along with earlier work (25, 60, 61) support the idea that a subset of these molecules can access the cytoplasmic steps of peptidoglycan synthesis. Depending on the specific probe and species of interest, D-amino acid labeling may be a read-out for multiple metabolic pathways.

We did not know *a priori* how closely the sites of L,D-transpeptidase activity would correspond to sites of peptidoglycan synthesis. Earlier work had suggested that D-alanine-D-alanine dipeptide probes are incorporated into peptidoglycan via an intracellular, MurF-dependent route (27, 44), theoretically offering a more specific way to label synthesis of the biopolymer. In direct support of a cytoplasmic uptake pathway, we show here that such probes rescue the growth of a DdlA mutant (**Fig. 3B**) and incorporate into lipid-linked peptidoglycan precursors (**Figs. 4B, 4C**).

Unexpectedly, labeling by alkDADA decreased in the absence of L,D-transpeptidases (**Fig. 5A**). Unlike the monopeptide probes, however, alkDADA-derived fluorescence was stable to pre-treatment with imipenem, an antibiotic that targets this class of enzymes ((63), **Figs. 2B, 2D**). Our data are most consistent with a model in which D,D-carboxypeptidases cleave a small proportion of alkDADA prior to incorporation and release D-alanine and alkDA. While the classic model substrate for *in vitro* assays of D,D-carboxypeptidase activity is the tripeptide Ac_2-L-lys-D-ala-D-ala, some D,D-carboxypeptidases retain low but measurable activity against the dipeptide Ac-D-ala-D-ala (71). We propose that, in *M. smegmatis*, apparent peptidoglycan labeling by alkDADA is a combination of: 1. intracellular alkDADA incorporation via MurF (**Figs. 3, 4B**), 2. extracellular alkDA incorporation by L,D-transpeptidases (**Figs. 2B, 2E**), and 3. more limited intracellular alkDA incorporation by DdlA/MurF (**Figs. 2B, 2E**). This model unites the following observations. First, alkDADA labeling in the *ΔldtABE* background is rescued by ampicillin or imipenem in a non-additive fashion (**Fig. 5C**). These antibiotics inhibit mycobacterial D,D-carboxypeptidases (63, 72) in addition to their transpeptidase targets. Second, 2 mM alkDADA

almost completely rescues the growth of Δ*alr* whereas 4 mM of the same compound only partially supports that of *ddlA*^{ts} strain (**Fig. 3**). Since Δ*alr* (but not *ddlA*^{ts}) grows like wildtype *M. smegmatis* in 200 μM D-alanine, one explanation for these data is that alkDADA-treated samples contain low levels of exogenous D-alanine. Third, mycobacteria are labeled at very low concentrations of monopeptide probe. Incubation of *M. smegmatis* with 1-2 μM alkDA yields comparable fluorescence to labeling with 2 mM alkDADA (**Fig. S9**). alkDA tagging decreases both in the presence of imipenem and in the absence of LdtABE (**Figs. 2B, 2E**). Therefore, low levels of alkDA in alkDADA-treated samples could make a substantial contribution to overall labeling, and could additionally explain the sensitivity of apparent alkDADA labeling to loss of L,D-transpeptidases (**Fig. 5A**).

Pre-incorporation cleavage of alkDADA by D,D-carboxypeptidases offers the most parsimonious explanation for the above observations. Unmodified DADA dipeptide has been reported to be a donor substrate for periplasmic exchange by an L,D transpeptidase purified from *Enterococcus faecalis* (73) but not from *Vibrio cholera*e (60). The discrepancy in alkDADA labeling phenotype from cells treated with imipenem (**Figs. 2B, 2D**) or lacking L,D-transpeptidases (**Fig. 5A**) suggests that the dipeptide is unlikely to be a direct substrate for these enzymes. Although we are unable to completely rule out abiotic degradation of alkDADA or trace contaminants carried over from alkDADA synthesis, neither potential source of unlabeled D-alanine and alkDA would be responsive to imipenem or ampicillin or explain the ability of these antibiotics to restore labeling in *ΔldtABE* (**Fig. 5C**). It is possible that imipenem and ampicillin have other, non-D,D-carboxypeptidase targets in common that account for the alkDADA rescue phenotype. Both of the drugs are likely to hinder D,D-transpeptidases, albeit to varying degrees (63), but a direct mechanism by which D,D-transpeptidase inhibition might enhance alkDADA labeling is not clear. By contrast, L,D-carboxypeptidases cut between the third and fourth positions of the muropeptide and could theoretically remove alkyne-bearing D-alanine residues from the stem

peptide. Although none of the five *M. tuberculosis* L,D-transpeptidases have this activity *in vitro* (64), the presence of tripeptide monomers in mycobacterial peptidoglycan (63, 74) suggests that the enzymes are likely to be present. However the sensitivity of L,D-carboxypeptidases to β-lactams is variable, positively correlates with the presence of a D-amino acid substituent, and requires relatively high concentrations of drug (~100 μM) for *in vitro* inhibition (75, 76). Neither imipenem nor meropenem have an amino acid side chain, and we have determined the MIC of imipenem for *M. smegmatis* to be ~1.6 μM. Meropenem treatment of *M. tuberculosis* up to 50 μM did not obviously change the proportion of tripeptide monomers (63), suggesting that L,D-carboxypeptidases, if active in mycobacteria, are unlikely to be inhibited by this or structurally-similar antibiotics. By contrast, D,D-carboxypeptidase sensitivity to carbapenems is clear: meropenem treatment of *M. tuberculosis* dramatically increases the proportion of pentapeptide monomers starting at 5 μM, and we likewise observe enhanced fluorescent vancomycin staining of *M. smegmatis* with 3.2 μM imipenem (**Fig. S8**). Inhibition of D,D-carboxypeptidases should not impact detection of alkDADA after it has incorporated into peptidoglycan, since these enzymes cleave the terminal D-alanine of the stem peptide and should spare the alkyne (which was initially at the N-terminus of alkDADA and is expected to occupy the fourth position of the muropeptide (27)). However inhibition of these enzymes prior to incorporation could halt the release of alkDA, very small amounts of which could influence overall labeling by alkDADA (**Fig. 5D**) as well as its sensitivity to L,D-transpeptidases (**Figs. 2B, 2E**).

One of the most striking differences between the peptidoglycan composition of mycobacteria and that of better-characterized species is the abundance of crosslinks generated by L,D-transpeptidation (74, 77). *M. smegmatis* is robustly labeled by 5-50 μM of most monopeptide probes whereas most other organisms require 250-1000 μM (42) to achieve similar qualitative results. This difference may largely reflect vigorous periplasmic exchange by some or all of the six L,D-transpeptidases encoded in the *M. smegmatis* genome. D,D-carboxypeptidase cleavage

of alkDADA is likely to be inefficient and release very limited amounts of alkDA (71). Such activity complicates the interpretation of alkDADA labeling because of the remarkable efficiency at which *M. smegmatis* is able to incorporate exogenous D-amino acids. If true, we expect that it may be a liability for other bacterial species with high L,D-transpeptidase activity.

The stem peptide of peptidoglycan is an active site of remodeling. Our finding that labeling by both monopeptide and dipeptide D-amino acid probes is susceptible to such remodeling underscores the idea that these reagents are not one-size-fits-all. The details of incorporation pathways differ between species and according to the specific chemical structure of the probe *e.g.* the appended fluorophore or chemical tag ((24, 60), **Figs. 2B, 2D, 2E**). If such parameters are known, D-amino acid probe labeling can potentially be used to query multiple metabolic processes in parallel. Conversely if a less complex readout is desired, N-acetylmuramic acid-based probes mark the glycan backbone of the biopolymer via a defined, engineered salvage pathway and are less susceptible to periplasmic remodeling (78).

Here we used D-amino acid probes to demonstrate that active cell envelope metabolism occurs in asymmetric polar gradients along the mycobacterial cell (**Fig. 1**). The cell periphery is not known to support surface expansion in these organisms ((3-9), **Fig. S6**). Accordingly, we sought to characterize the molecular processes that underlie the labeling patterns. Since a subset of the monopeptide probes is incorporated almost entirely by L,D-transpeptidases (**Figs. 2B, 2D, 2E, 5A, 5B**), we infer that these enzymes have the capacity to act along the sidewall. The dipeptide probes access the cytoplasmic steps of precursor synthesis (**Figs. 3B, 4B, 4C**). Although alkDADA was sensitive to L,D-transpeptidation (**Fig. 5A**), inhibition of periplasmic remodeling by imipenem did not diminish its ability to mark the mycobacterial sidewall (**Fig. 5D**). We surmise that lipid-linked peptidoglycan precursors are also synthesized at both polar and

lateral sites. In support, MurG fused to two different fluorescent proteins and expressed under two different promoters is present in these locations (22).

Our standard experimental protocol for detecting envelope labeling is to perform CuAAC on fixed cells. Because formaldehyde fixation can permeabilize the plasma membrane to small molecules, fluorescently-labeled material may be intracellular, extracellular or both. Dipeptide labeling (in the presence of imipenem, (**Fig. 5D**)) could therefore be a readout for lipid I/II on the cytoplasmic face of the plasma membrane, uncrosslinked lipid II on the periplasmic side, or polymerized peptidoglycan. Differentiating between these possibilities would help inform a model for the physiological role of precursor synthesis along the mycobacterial sidewall. Two lines of evidence suggest that the lipid precursors are used to build the peptidoglycan polymer. First, fluorescent vancomycin stains both the poles and periphery of the mycobacterial cell ((8), **Fig. S2**). At least a proportion of the uncrosslinked pentapeptides bound by this reagent is lipid II. Since vancomycin does not normally cross the plasma membrane, this observation suggests that both the polar and sidewall precursors are likely to be flipped to the periplasm. Second, fluorescent PonA1 fusions and β-lactam labeling demonstrate that pencillin-binding proteins are active at both the poles and the sidewall ((9, 19, 21, 51), **Fig. S1**). The presence of pencillin-binding protein activity indicates that these sites are competent for assembly of the crosslinked biopolymer. Taken together our data suggest that precursors are unlikely to be stored along the mycobacterial sidewall, but rather that they actively contribute to the periplasmic assembly of peptidoglycan.

Assembly of the three, covalently-bound layers of the mycobacterial envelope—peptidoglycan, arabinogalactan and the mycomembrane—has long been presumed to be spatially coincident. In support, metabolic labeling of the mycomembrane is enriched at mycobacterial cell tips but present along lateral surfaces ((36), **Fig. 1**). However we previously helped to show that

fluorescent protein fusions to terminal synthetic enzymes for peptidoglycan, arabinogalactan and mycolic acid synthesis are mobile and colocalize at subpolar regions but not along the sidewall (5). It may be that mycobacterial cell expansion occurs only when the synthesis of different cell envelope precursors is concentrated or coordinated in some fashion. Alternatively, or additionally, concentration or coordination of precursor synthesis may require cell growth.

Although the lateral surface of mycobacteria does not appear to contribute to cell elongation under normal growth conditions (**Fig. S6**), it nevertheless hosts a substantial portion of measurable envelope synthesis and remodeling. The intracellular difference in signal between the poles reflected relative elongation rates, as the RADA-bright cell tip, which coincides with the alkDADA- and OalkTMM-bright cell tip (**Fig. 1B**) grows faster than the RADA-dim cell tip (**Fig. S6**). If we arbitrarily define the slow polar region as the dimmer, first 25% of the cell length, the sidewall to be the middle 50%, and the fast polar region to be the brighter, final 25%, the distribution of alkDADA, OalkTMM, RADA or HADA labeling in non-septating *M. smegmatis* is approximately 15-25% at the slow pole; 30-40% along the sidewall; 40-50% at the fast pole (**Figs. 2C, 2D,** top). The 2-3-fold ratio of fast:slow pole fluorescence roughly corresponds to previous estimates of intracellular differences in polar elongation (3, 9). We find that the distribution of HADA labeling in *M. tuberculosis* is shifted away from the fast pole towards the periphery, with a ratio of 20:50:30 for slow pole:sidewall:fast pole (**Fig. 2D**). Diminished polarity and asymmetry is also apparent in the sub-population of *M. tuberculosis* that is labeled by alkDADA and OalkTMM (**Fig. S5C**). Our data are in agreement with the heterogeneity in polar dominance observed previously for *M. tuberculosis* (39). Although we cannot rule out a contribution from cyan autofluorescence, these experiments also suggest that sidewall envelope metabolism may be even more prominent in *M. tuberculosis* than in *M. smegmatis*, comprising half of the total cell output.

What is the physiological role for envelope metabolism that does not directly contribute to physical expansion of the cell surface? It is possible that envelope assembly along the lateral surface of the mycobacterial cell is simply a byproduct of synthetic enzymes that are en route to the (polar or subpolar) elongasome or the divisome. Having active enzymes “at the ready” could enable efficient coordination between cell growth and septation. We think that this model is less likely, however, given the energetic cost of producing complex macromolecules and the known limits on the steady-state pools of lipid-linked peptidoglycan precursors (79). Instead we propose that envelope metabolism along the sidewall could allow mycobacteria to edit what would otherwise be an inert surface. Peptidoglycan and mycomembrane synthesis in this region may thicken or fill in the gaps of envelope that was initially deposited at the poles or the septum and enable the bacterium to correct stochastic defects, repair damage and promote nutrient uptake. More broadly, the ability to tailor the entire cell surface, not just the ends, should enable more rapid adaptation to external stimuli. Such activity may be particularly important for *M. tuberculosis*, a slow-growing organism that must survive a hostile, nutrient-poor environment.

Materials and Methods

Bacterial strains and culture conditions. mc^{2}155 *M. smegmatis* and Δ*RD1* Δ*panCD M. tuberculosis* (80) were grown at 37 °C in Middlebrook 7H9 growth medium (BD Difco, Franklin Lakes, NJ) supplemented with glycerol, Tween 80 and ADC (*M. smegmatis*) or OADC and 50 µg/ml pantothenic acid (*M. tuberculosis*). The Δ*alr* strain was further supplemented with 1 mM D-alanine. The *ddlA*^{ts} strain was grown in 7H9-ADC at 30 °C or 37 °C as specified. Strains are detailed in **Table S1**.

Cell envelope labeling. Probes used in this study include (i) fluorescent D-amino acids HADA, NADA and RADA (Tocris Bioscience, Bristol, United Kingdom) (ii) alkDA (R-propargylglycine,

Thermo Fisher, Waltham, MA) (iii) alkDADA and azDADA (Chemical Synthesis Core Facility, Albert Einstein College of Medicine, Bronx, NY) and (iv) OalkTMM and NalkTMM, synthesized as described previously (33). The labeling procedures were performed with modifications from (13, 25, 33). Unless otherwise indicated, mid-log *M. smegmatis* or *M. tuberculosis* were labeled with 500 µM HADA, 25 µM NADA or RADA, 50 µM alkDA, 1 or 2 mM alkDADA, 50 µM OalkTMM or 250 µM NalkTMM for 15 min or 2 hours, respectively. In some cases *M. smegmatis* was preincubated +/- antibiotics at 2X MIC (160 µg/mL D-cycloserine, 16 µg/mL ampicillin (with 5 µg/mL clavulanate), 1 µg/mL imipenem (with 5 µg/mL clavulanate), 12 µg/mL vancomycin) for 30 min then grown for an additional 15 min in the presence of the probes. Cultures were then centrifuged at 4 °C, washed in pre-chilled PBS containing 0.05% Tween 80 and 0.01% BSA (PBSTB) and fixed for 10 min in 2% formaldehyde at room temperature (RT). After two washes in PBSTB, the bacterial pellets were resuspended in half of the original volume of freshly-prepared CuAAC solution in PBSTB (25) containing either AF488 picolyl azide or carboxyrhodamine 110 azide (Click Chemistry Tools, Scottsdale, AZ) or 3-azido-7-hydroxycoumarin (Jena Biosciences, Jena, Germany). For *M. tuberculosis* experiments and in **Fig. S4A**, we used a modified, low-copper CuAAC reaction protocol: 200 µM $CuSO_4$ and 800 µM BTTP (Chemical Synthesis Core Facility, Albert Einstein College of Medicine, Bronx, NY) were pre-mixed then added to PBSTB. Immediately before resuspending the pellets, 2.5 mM freshly prepared sodium ascorbate and 300 µM 3-azido-7-hydroxycoumarin were added to the mixture. After 30-60 min gentle agitation at RT, cultures were washed once with PBSTB, once with PBS and resuspended in PBS for imaging or flow cytometry analysis (FITC, BV510, and Texas Red channels on a BD DUAL LSRFortessa, UMass Amherst Flow Cytometry Core Facility). NHS ester dye labeling and fluorescent vancomycin labeling were performed as described (3, 6). *M. tuberculosis* was post-fixed with 4% formaldehyde overnight at RT prior to removing from the biosafety cabinet. For Bocillin labeling experiments, 500 µL of mid-log *M. smegmatis* was washed once in PBST and resuspended in PBST containing 5 µg/mL

clavulanate. Bacteria were then pre-incubated or not with 50 µg/mL ampicillin or D-cycloserine at RT with gentle agitation. After 15 min, 50 µg/mL Bocillin FL (Thermo Fisher) was added and cultures were incubated for an additional 30 min. They were then washed three times in PBST and imaged live on agar pads.

Genetic manipulation. The *Δalr M. smegmatis* strain was generated using standard recombineering methods (81, 82). 500 bp up and downstream of *alr* were cloned on either side of the *hyg*^{R} cassette flanked with *loxP* sites. After induction of *recET*, transformation and subsequent selection on hygromycin and 1 mM D-alanine, PCR was used to confirm the presence of the correct insert. Strains were then cured of the *hyg*^{R} cassette by transformation with an episomal plasmid carrying the Cre recombinase and a sucrose negative selection marker. Strains were cured of this plasmid by repeated passaging in the presence of sucrose.

M.smegmatis lacking *ldtA, ldtB* and/or *ldtE* were generously provided by Dr. Kasia Baranowski and Dr. Eric Rubin (described in a separate manuscript). Briefly, strains were constructed by recombineering to replace the endogenous copies with zeocin or hygromycin resistance cassettes flanked by *loxP* sites as previously described above (38). Once the knock-outs were verified by PCR, the antibiotic resistance cassettes were removed by the expression of Cre recombinase. To complement Δ*ldtABE,* a copy of *ldtA* was under the constitutive TetO promoter on a kanamycin marked vector (CT94) that integrates at the L5 phage integration site of the chromosome.

Microscopy. Fixed bacteria were imaged either by conventional fluorescence microscopy (Nikon Eclipse E600, Nikon Eclipse Ti or Zeiss Axioscope A1 with 100x objectives) or by structured illumination microscopy (Nikon SIM-E/A1R with SR Apo TIRF 100x objective). Time-

lapse microscopy was performed on an inverted Nikon TI-E microscope at 60x magnification using a CellAsicB04A plate with continuously flowed 7H9 medium in a 37 °C chamber.

Microscopy analysis. Images were processed using FIJI (83) and cells were outlined and segmented using Oufti (84). Fluorescence signals of each cell were detected using Oufti and analyzed using custom-written MATLAB codes. The fluorescence intensities that we report here have been normalized by cell area. We distinguished septating from non-septating cells using the probe fluorescence profile along the long cell axis. We used the peakfinderprogram (85) to identify peaks in the labeling profile. Because our probes label both the cell poles as well as the septum, septating cells were those that had three peaks in their labeling profile, with the middle peak positioned between 30% and 70% along the normalized long cell axis. Non-septating cells were identified as having only two peaks.

Detection of lipid-linked peptidoglycan precursors. To detect endogenous lipid-linked peptidoglycan precursors, we adopted the assay developed in (67) with some modifications. *M. smegmatis* was inoculated in 100 mL of 7H9 medium and grown to mid-log phase at 37 ºC. Where applicable, MurJ was depleted by 8 hours of anhydrotetracycline-induced protein degradation as described (70). The bacteria were then divided into 25 mL cultures that were subjected or not to freshly-prepared 80 µg/mL vancomycin and/or 10 µg/mL D-cycloserine. After one hour of incubation at 37 ºC, bacteria were collected by centrifugation and cell pellets were normalized by wet weight. 200-300 mg wet pellet was resuspended in 500 µL 1% glacial acetic acid in water. 500 µL of the resuspended pellet mixture was transferred into a vial containing 500 µL of chloroform and 1 mL of methanol and kept at room temperature for 1-2 hours with occasional vortexing. The mixture was then centrifuged at 21,000x g for 10 min at RT and the supernatant was transferred into a vial containing 500 µL of 1% glacial acetic acid in water and 500 µL chloroform, and vortexed for 1 min. After centrifugation at 900x g for 2 min at RT, three

phases were distinguishable: aqueous, an interface, and organic. We collected the lipids from the organic phase and from the interface and concentrated it under nitrogen. Organic extracts were resuspended in 12 µL of DMSO and then incubated with purified *S. aureus* PBP4 and biotin-D-lysine (BDL; Chem-Impex International) as described (67). Upon completion of the BDL exchange reaction, 10 µL of 2X loading buffer was added to the vials. Contents were boiled at 95 ºC for 5 min then run on an 18% SDS polyacrylamide gel. Biotinylated species were transferred to a PVDF membrane, blotted with streptavidin-HRP (diluted 1:10,000, Thermo-Fisher) and visualized in an ImageQuant system (GE Healthcare).

To detect lipid-linked precursors that had been metabolically labeled with alkDADA or azDADA, growth of the *Δalr* strain was initially supported by the inclusion of 2 mM D-alanine D-alanine (Sigma-Aldrich) in the 7H9 medium. *Δalr* bacteria were harvested and washed twice in sterile PBS + 0.05% Tween-80 prior to resuspension in 100 mL of pre-warmed medium. Both wildtype and *Δalr M. smegmatis* were incubated in 0.5-1 mM of alkDADA or azDADA for 1 hour then harvested as described above. Organic extracts from metabolically-labeled cultures were subjected to CuAAC reaction by adding, in order and in a non-stick vial: 2 µL of PBS + 0.05% Tween-80, 1 µL of 5 mM $CuSO_4$, 1 µL of 20 mM BTTP, 1 µL of freshly-prepared 50 mM sodium ascorbate, 3 µL of 10 mM picolyl azide biotin or alkyne biotin (Click Chemistry Tools), and 2 µL of the organic extract. The reaction was incubated for one hour at RT with gentle shaking prior to detecting as above.

Funding information

MSS is supported by NIH U01CA221230 and NIH DP2 AI138238. ESM is supported by NIH T32 GM008515 administered to the Chemistry Biology Interface Program at the University of Massachuetts Amherst. BMS is supported by a Research Corporation for Science Advancement

Cottrell College Science Award 22525. HCL is the recipient of a Life Sciences Research Foundation Fellowship sponsored by the Simons Foundation. The funders had no role in study design, data collection and interpretation, or the decision to submit the work for publication.

Acknowledgments

We are grateful to Dr. Kasia Baranowski, Dr. Hesper Rego and Dr. Eric Rubin for sharing L,D-transpeptidase mutants and for providing critical feedback. We thank Dr. Suzanne Walker and Dr. Kaitlin Schaefer for the *S. aureus pbp4* expression construct and for helpful technical advice; Dr. Steven Sandler, Dr. Peter Chien, Dr. James Chambers and Dr. Amy Burnside for microscopy and flow cytometry guidance; Ms. Sylvia Rivera for technical assistance. We also acknowledge Dr. Chris Sassetti for the *murJ* depletion strain, Dr. Graham Hatfull for the *ddlA*^{ts} mutant, Dr. William Jacobs for *ΔRD1* Δ*panCD M. tuberculosis* and Dr. Yves Brun, Dr. Erkin Kuru and Dr. Michael VanNieuwenhze for the initial supply of the alkDADA (EDA-DA) probe.

References

1. de Pedro MA, Quintela JC, Holtje JV, Schwarz H. 1997. Murein segregation in *Escherichia coli*. Journal of Bacteriology 179:2823-2834.
2. Daniel RA, Errington J. 2003. Control of cell morphogenesis in bacteria: two distinct ways to make a rod-shaped cell. Cell 113:767-776.
3. Aldridge BB, Fernandez-Suarez M, Heller D, Ambravaneswaran V, Irimia D, Toner M, Fortune SM. 2012. Asymmetry and aging of mycobacterial cells lead to variable growth and antibiotic susceptibility. Science 335:100-104.

4. Santi I, Dhar N, Bousbaine D, Wakamoto Y, McKinney JD. 2013. Single-cell dynamics of the chromosome replication and cell division cycles in mycobacteria. Nature Communications 4:2470.

5. Meniche X, Otten R, Siegrist MS, Baer CE, Murphy KC, Bertozzi CR, Sassetti CM. 2014. Subpolar addition of new cell wall is directed by DivIVA in mycobacteria. PNAS U S A 111:E3243-3251.

6. Thanky NR, Young DB, Robertson BD. 2007. Unusual features of the cell cycle in mycobacteria: polar-restricted growth and the snapping-model of cell division. Tuberculosis 87:231-236.

7. Kieser KJ, Rubin EJ. 2014. How sisters grow apart: mycobacterial growth and division. Nature Reviews Microbiology 12:550-562.

8. Singh B, Nitharwal RG, Ramesh M, Pettersson BM, Kirsebom LA, Dasgupta S. 2013. Asymmetric growth and division in Mycobacterium spp.: compensatory mechanisms for non-medial septa. Molecular Microbiology 88:64-76.

9. Joyce G, Williams KJ, Robb M, Noens E, Tizzano B, Shahrezaei V, Robertson BD. 2012. Cell division site placement and asymmetric growth in mycobacteria. PloS ONE 7:e44582.

10. Fenton AK, Gerdes K. 2013. Direct interaction of FtsZ and MreB is required for septum synthesis and cell division in *Escherichia coli.* The EMBO Journal 32:1953-1965.

11. van der Ploeg R, Verheul J, Vischer NO, Alexeeva S, Hoogendoorn E, Postma M, Banzhaf M, Vollmer W, den Blaauwen T. 2013. Colocalization and interaction between elongasome and divisome during a preparative cell division phase in *Escherichia coli.* Molecular Microbiology 87:1074-1087.

12. Brown PJ, de Pedro MA, Kysela DT, Van der Henst C, Kim J, De Bolle X, Fuqua C, Brun YV. 2012. Polar growth in the Alphaproteobacterial order Rhizobiales. PNAS U S A 109:1697-1701.

13. Kuru E, Hughes HV, Brown PJ, Hall E, Tekkam S, Cava F, de Pedro MA, Brun YV, VanNieuwenhze MS. 2012. In Situ probing of newly synthesized peptidoglycan in live bacteria with fluorescent D-amino acids. Angewandte Chemie 51:12519-12523.

14. Zupan JR, Cameron TA, Anderson-Furgeson J, Zambryski PC. 2013. Dynamic FtsA and FtsZ localization and outer membrane alterations during polar growth and cell division in Agrobacterium tumefaciens. PNAS U S A 110:9060-9065.

15. Jankute M, Cox JA, Harrison J, Besra GS. 2015. Assembly of the Mycobacterial Cell Wall. Annual Review of Microbiology 69:405-423.

16. Hayashi JM, Luo CY, Mayfield JA, Hsu T, Fukuda T, Walfield AL, Giffen SR, Leszyk JD, Baer CE, Bennion OT, Madduri A, Shaffer SA, Aldridge BB, Sassetti CM, Sandler SJ, Kinoshita T, Moody DB, Morita YS. 2016. Spatially distinct and metabolically active membrane domain in mycobacteria. PNAS U S A 113:5400-5405.

17. Hayashi JM, Richardson K, Melzer ES, Sandler SJ, Aldridge BB, Siegrist MS, Morita YS. 2018. Stress-Induced Reorganization of the Mycobacterial Membrane Domain. mBio 9.

18. Carel C, Nukdee K, Cantaloube S, Bonne M, Diagne CT, Laval F, Daffe M, Zerbib D. 2014. Mycobacterium tuberculosis proteins involved in mycolic acid synthesis and transport localize dynamically to the old growing pole and septum. PloS ONE 9:e97148.

19. Hett EC, Chao MC, Rubin EJ. 2010. Interaction and modulation of two antagonistic cell wall enzymes of mycobacteria. PLoS Pathogens 6:e1001020.

20. Kieser KJ, Boutte CC, Kester JC, Baer CE, Barczak AK, Meniche X, Chao MC, Rego EH, Sassetti CM, Fortune SM, Rubin EJ. 2015. Phosphorylation of the Peptidoglycan Synthase PonA1 Governs the Rate of Polar Elongation in Mycobacteria. PLoS Pathogens 11:e1005010.

21. Plocinski P, Ziolkiewicz M, Kiran M, Vadrevu SI, Nguyen HB, Hugonnet J, Veckerle C, Arthur M, Dziadek J, Cross TA, Madiraju M, Rajagopalan M. 2011. Characterization of

CrgA, a new partner of the *Mycobacterium tuberculosis* peptidoglycan polymerization complexes. Journal of Bacteriology 193:3246-3256.

22. Meniche X, Otten R, Siegrist MS, Baer CE, Murphy KC, Bertozzi CR, Sassetti CM. 2014. Subpolar addition of new cell wall is directed by DivIVA in mycobacteria. PNAS U S A.

23. Michaelis AM, Gitai Z. 2010. Dynamic polar sequestration of excess MurG may regulate enzymatic function. Journal of Bacteriology 192:4597-4605.

24. Siegrist MS, Swarts BM, Fox DM, Lim SA, Bertozzi CR. 2015. Illumination of growth, division and secretion by metabolic labeling of the bacterial cell surface. FEMS Microbiology Reviews 39:184-202.

25. Siegrist MS, Whiteside S, Jewett JC, Aditham A, Cava F, Bertozzi CR. 2013. D-amino acid chemical reporters reveal peptidoglycan dynamics of an intracellular pathogen. ACS Chemical Biology 8:500-505.

26. Lebar MD, May JM, Meeske AJ, Leiman SA, Lupoli TJ, Tsukamoto H, Losick R, Rudner DZ, Walker S, Kahne D. 2014. Reconstitution of peptidoglycan cross-linking leads to improved fluorescent probes of cell wall synthesis. JACS 136:10874-10877.

27. Liechti GW, Kuru E, Hall E, Kalinda A, Brun YV, VanNieuwenhze M, Maurelli AT. 2014. A new metabolic cell-wall labelling method reveals peptidoglycan in *Chlamydia trachomatis*. Nature 506:507-510.

28. Pidgeon SE, Fura JM, Leon W, Birabaharan M, Vezenov D, Pires MM. 2015. Metabolic Profiling of Bacteria by Unnatural C-terminated D-Amino Acids. Angewandte Chemie 54:6158-6162.

29. Dumont A, Malleron A, Awwad M, Dukan S, Vauzeilles B. 2012. Click-mediated labeling of bacterial membranes through metabolic modification of the lipopolysaccharide inner core. Angewandte Chemie 51:3143-3146.

30. Mas Pons J, Dumont A, Sautejeau G, Fugier E, Baron A, Dukan S, Vauzeilles B. 2014. Identification of living *Legionella pneumophila* using species-specific metabolic lipopolysaccharide labeling. Angewandte Chemie 53:1275-1278.

31. Backus KM, Boshoff HI, Barry CS, Boutureira O, Patel MK, D'Hooge F, Lee SS, Via LE, Tahlan K, Barry CE, 3rd, Davis BG. 2011. Uptake of unnatural trehalose analogs as a reporter for *Mycobacterium tuberculosis*. Nature Chemical Biology 7:228-235.

32. Swarts BM, Holsclaw CM, Jewett JC, Alber M, Fox DM, Siegrist MS, Leary JA, Kalscheuer R, Bertozzi CR. 2012. Probing the mycobacterial trehalome with bioorthogonal chemistry. JACS 134:16123-16126.

33. Foley HN, Stewart JA, Kavunja HW, Rundell SR, Swarts BM. 2016. Bioorthogonal Chemical Reporters for Selective In Situ Probing of Mycomembrane Components in Mycobacteria. Angewandte Chemie 55:2053-2057.

34. Kolbe K, Mockl L, Sohst V, Brandenburg J, Engel R, Malm S, Brauchle C, Holst O, Lindhorst TK, Reiling N. 2017. Azido pentoses: A New Tool to Efficiently Label *Mycobacterium tuberculosis* Clinical Isolates. Chembiochem.

35. Rundell SR, Wagar ZL, Meints LM, Olson CD, O'Neill MK, Piligian BF, Poston AW, Hood RJ, Woodruff PJ, Swarts BM. 2016. Deoxyfluoro-d-trehalose (FDTre) analogues as potential PET probes for imaging mycobacterial infection. Organic & Biomolecular Chemistry 14:8598-8609.

36. Rodriguez-Rivera FP, Zhou X, Theriot JA, Bertozzi CR. 2017. Visualization of mycobacterial membrane dynamics in live cells. JACS 139:3488-3495.

37. Lebar MD, May JM, Meeske AJ, Leiman SA, Lupoli TJ, Tsukamoto H, Losick R, Rudner DZ, Walker S, Kahne D. 2014. Reconstitution of Peptidoglycan Cross-Linking Leads to Improved Fluorescent Probes of Cell Wall Synthesis. JACS.

38. Boutte CC, Baer CE, Papavinasasundaram K, Liu W, Chase MR, Meniche X, Fortune SM, Sassetti CM, Ioerger TR, Rubin EJ. 2016. A cytoplasmic peptidoglycan amidase homologue controls mycobacterial cell wall synthesis. eLife 5.

39. Botella H, Yang G, Ouerfelli O, Ehrt S, Nathan CF, Vaubourgeix J. 2017. Distinct Spatiotemporal Dynamics of Peptidoglycan Synthesis between *Mycobacterium smegmatis* and *Mycobacterium tuberculosis*. mBio 8.

40. Schubert K, Sieger B, Meyer F, Giacomelli G, Bohm K, Rieblinger A, Lindenthal L, Sachs N, Wanner G, Bramkamp M. 2017. The Antituberculosis Drug Ethambutol Selectively Blocks Apical Growth in CMN Group Bacteria. mBio 8.

41. de Pedro MA, Cava F. 2015. Structural constraints and dynamics of bacterial cell wall architecture. Frontiers in Microbiology 6:449.

42. Kuru E, Tekkam S, Hall E, Brun YV, Van Nieuwenhze MS. 2015. Synthesis of fluorescent D-amino acids and their use for probing peptidoglycan synthesis and bacterial growth in situ. Nature Protocols 10:33-52.

43. Glauner B, Holtje JV. 1990. Growth pattern of the murein sacculus of *Escherichia coli.* The Journal of Biological Chemistry 265:18988-18996.

44. Sarkar S, Libby EA, Pidgeon SE, Dworkin J, Pires MM. 2016. In Vivo Probe of Lipid II-Interacting Proteins. Angewandte Chemie 55:8401-8404.

45. Boyce M, Carrico IS, Ganguli AS, Yu SH, Hangauer MJ, Hubbard SC, Kohler JJ, Bertozzi CR. 2011. Metabolic cross-talk allows labeling of O-linked beta-N-acetylglucosamine-modified proteins via the N-acetylgalactosamine salvage pathway. PNAS U S A108:3141-3146.

46. Qin W, Qin K, Fan X, Peng L, Hong W, Zhu Y, Lv P, Du Y, Huang R, Han M, Cheng B, Liu Y, Zhou W, Wang C, Chen X. 2017. Artificial Cysteine S-Glycosylation Induced by Per-O-Acetylated Unnatural Monosacharides during Metabolic Glycan Labeling. Angewandte Chemie.

47. Zhao H, Patel V, Helmann JD, Dorr T. 2017. Don't let sleeping dogmas lie: new views of peptidoglycan synthesis and its regulation. Molecular Microbiology 106:847-860.

48. Cho H, Wivagg CN, Kapoor M, Barry Z, Rohs PD, Suh H, Marto JA, Garner EC, Bernhardt TG. 2016. Bacterial cell wall biogenesis is mediated by SEDS and PBP polymerase families functioning semi-autonomously. Nature Microbiology:16172.

49. Leclercq S, Derouaux A, Olatunji S, Fraipont C, Egan AJ, Vollmer W, Breukink E, Terrak M. 2017. Interplay between Penicillin-binding proteins and SEDS proteins promotes bacterial cell wall synthesis. Scientific Reports 7:43306.

50. Meeske AJ, Riley EP, Robins WP, Uehara T, Mekalanos JJ, Kahne D, Walker S, Kruse AC, Bernhardt TG, Rudner DZ. 2016. SEDS proteins are a widespread family of bacterial cell wall polymerases. Nature 537:634-638.

51. Kieser KJ, Baranowski C, Chao MC, Long JE, Sassetti CM, Waldor MK, Sacchettini JC, Ioerger TR, Rubin EJ. 2015. Peptidoglycan synthesis in *Mycobacterium tuberculosis* is organized into networks with varying drug susceptibility. PNAS U S A 112:13087-13092.

52. Landgraf D, Okumus B, Chien P, Baker TA, Paulsson J. 2012. Segregation of molecules at cell division reveals native protein localization. Nature Methods 9:480-482.

53. Kocaoglu O, Carlson EE. 2013. Penicillin-binding protein imaging probes. Current Protocols in Chemical Biology 5:239-250.

54. Liechti GW, Kuru E, Hall E, Kalinda A, Brun YV, Vannieuwenhze M, Maurelli AT. 2013. A new metabolic cell-wall labelling method reveals peptidoglycan in *Chlamydia trachomatis*. Nature.

55. Mahal LK, Yarema KJ, Bertozzi CR. 1997. Engineering chemical reactivity on cell surfaces through oligosaccharide biosynthesis. Science 276:1125-1128.

56. Yang M, Jalloh AS, Wei W, Zhao J, Wu P, Chen PR. 2014. Biocompatible click chemistry enabled compartment-specific pH measurement inside *E. coli.* Nature Communications 5:4981.

57. Hancock IC, Carman S, Besra GS, Brennan PJ, Waite E. 2002. Ligation of arabinogalactan to peptidoglycan in the cell wall of *Mycobacterium smegmatis* requires concomitant synthesis of the two wall polymers. Microbiology 148:3059-3067.

58. Wang W, Hong S, Tran A, Jiang H, Triano R, Liu Y, Chen X, Wu P. 2011. Sulfated ligands for the copper(I)-catalyzed azide-alkyne cycloaddition. Chemistry 6:2796-2802.

59. Patino S, Alamo L, Cimino M, Casart Y, Bartoli F, Garcia MJ, Salazar L. 2008. Autofluorescence of mycobacteria as a tool for detection of *Mycobacterium tuberculosis*. Journal of Clinical Microbiology 46:3296-3302.

60. Cava F, de Pedro MA, Lam H, Davis BM, Waldor MK. 2011. Distinct pathways for modification of the bacterial cell wall by non-canonical D-amino acids. The EMBO Journal 30:3442-3453.

61. Ngo JT, Adams SR, Deerinck TJ, Boassa D, Rodriguez-Rivera F, Palida SF, Bertozzi CR, Ellisman MH, Tsien RY. 2016. Click-EM for imaging metabolically tagged nonprotein biomolecules. Nature Chemical Biology 12:459-465.

62. Feng Z, Barletta RG. 2003. Roles of *Mycobacterium smegmatis* D-alanine:D-alanine ligase and D-alanine racemase in the mechanisms of action of and resistance to the peptidoglycan inhibitor D-cycloserine. Antimicrobial Agents and Chemotherapy 47:283-291.

63. Kumar P, Arora K, Lloyd JR, Lee IY, Nair V, Fischer E, Boshoff HI, Barry CE, 3rd. 2012. Meropenem inhibits D,D-carboxypeptidase activity in *Mycobacterium tuberculosis*. Molecular Microbiology 86:367-381.

64. Cordillot M, Dubee V, Triboulet S, Dubost L, Marie A, Hugonnet JE, Arthur M, Mainardi JL. 2013. In vitro cross-linking of *Mycobacterium tuberculosis* peptidoglycan by L,D-transpeptidases and inactivation of these enzymes by carbapenems. Antimicrobial Agents and Chemotherapy 57:5940-5945.

65. Barreteau H, Kovac A, Boniface A, Sova M, Gobec S, Blanot D. 2008. Cytoplasmic steps of peptidoglycan biosynthesis. FEMS Microbiology Reviews 32:168-207.

66. Belanger AE, Porter JC, Hatfull GF. 2000. Genetic analysis of peptidoglycan biosynthesis in mycobacteria: characterization of a *ddlA* mutant of *Mycobacterium smegmatis*. Journal of Bacteriology 182:6854-6856.

67. Qiao Y, Lebar MD, Schirner K, Schaefer K, Tsukamoto H, Kahne D, Walker S. 2014. Detection of lipid-linked peptidoglycan precursors by exploiting an unexpected transpeptidase reaction. JACS 136:14678-14681.

68. Qiao Y, Srisuknimit V, Rubino F, Schaefer K, Ruiz N, Walker S, Kahne D. 2017. Lipid II overproduction allows direct assay of transpeptidase inhibition by beta-lactams. Nature Chemical Biology 13:793-798.

69. Lee W, Schaefer K, Qiao Y, Srisuknimit V, Steinmetz H, Muller R, Kahne D, Walker S. 2016. The Mechanism of Action of Lysobactin. JACS 138:100-103.

70. Gee CL, Papavinasasundaram KG, Blair SR, Baer CE, Falick AM, King DS, Griffin JE, Venghatakrishnan H, Zukauskas A, Wei JR, Dhiman RK, Crick DC, Rubin EJ, Sassetti CM, Alber T. 2012. A phosphorylated pseudokinase complex controls cell wall synthesis in mycobacteria. Science Signaling 5:ra7.

71. Nieto M, Perkins HR, Leyh-Bouille M, Frere JM, Ghuysen JM. 1973. Peptide inhibitors of Streptomyces D,D-carboxypeptidases. The Biochemical Journal 131:163-171.

72. Eun HM, Yapo A, Petit JF. 1978. D,D-Carboxypeptidase activity of membrane fragments of *Mycobacterium smegmatis*. Enzymatic properties and sensitivity to beta-lactam antibiotics. European Journal of Biochemistry 86:97-103.

73. Magnet S, Arbeloa A, Mainardi JL, Hugonnet JE, Fourgeaud M, Dubost L, Marie A, Delfosse V, Mayer C, Rice LB, Arthur M. 2007. Specificity of L,D-transpeptidases from Gram-positive bacteria producing different peptidoglycan chemotypes. The Journal of Biological Chemistry 282:13151-13159.

74. Lavollay M, Arthur M, Fourgeaud M, Dubost L, Marie A, Veziris N, Blanot D, Gutmann L, Mainardi JL. 2008. The peptidoglycan of stationary-phase *Mycobacterium tuberculosis* predominantly contains cross-links generated by L,D-transpeptidation. Journal of Bacteriology 190:4360-4366.

75. Ursinus A, Steinhaus H, Holtje JV. 1992. Purification of a nocardicin A-sensitive L,D-carboxypeptidase from *Escherichia coli* by affinity chromatography. Journal of Bacteriology 174:441-446.

76. Templin MF, Ursinus A, Holtje JV. 1999. A defect in cell wall recycling triggers autolysis during the stationary growth phase of *Escherichia coli*. The EMBO Journal 18:4108-4117.

77. Lavollay M, Fourgeaud M, Herrmann JL, Dubost L, Marie A, Gutmann L, Arthur M, Mainardi JL. 2011. The peptidoglycan of *Mycobacterium abscessus* is predominantly cross-linked by L,D-transpeptidases. Journal of Bacteriology 193:778-782.

78. Liang H, DeMeester KE, Hou CW, Parent MA, Caplan JL, Grimes CL. 2017. Metabolic labelling of the carbohydrate core in bacterial peptidoglycan and its applications. Nature Communications 8:15015.

79. van Heijenoort Y, Gomez M, Derrien M, Ayala J, van Heijenoort J. 1992. Membrane intermediates in the peptidoglycan metabolism of *Escherichia coli*: possible roles of PBP 1b and PBP 3. Journal of Bacteriology 174:3549-3557.

80. Sambandamurthy VK, Derrick SC, Hsu T, Chen B, Larsen MH, Jalapathy KV, Chen M, Kim J, Porcelli SA, Chan J, Morris SL, Jacobs WR, Jr. 2006. *Mycobacterium tuberculosis ΔRD1 ΔpanCD*: a safe and limited replicating mutant strain that protects immunocompetent and immunocompromised mice against experimental tuberculosis. Vaccine 24:6309-6320.

81. van Kessel JC, Hatfull GF. 2007. Recombineering in *Mycobacterium tuberculosis.* Nature Methods 4:147-152.

82. Murphy KC, Papavinasasundaram K, Sassetti CM. 2015. Mycobacterial recombineering. Methods in Molecular Biology 1285:177-199.

83. Schindelin J, Arganda-Carreras I, Frise E, Kaynig V, Longair M, Pietzsch T, Preibisch S, Rueden C, Saalfeld S, Schmid B, Tinevez JY, White DJ, Hartenstein V, Eliceiri K, Tomancak P, Cardona A. 2012. Fiji: an open-source platform for biological-image analysis. Nature Methods 9:676-682.

84. Paintdakhi A, Parry B, Campos M, Irnov I, Elf J, Surovtsev I, Jacobs-Wagner C. 2016. Oufti: an integrated software package for high-accuracy, high-throughput quantitative microscopy analysis. Molecular Microbiology 99:767-777.

85. Sliusarenko O, Heinritz J, Emonet T, Jacobs-Wagner C. 2011. High-throughput, subpixel precision analysis of bacterial morphogenesis and intracellular spatio-temporal dynamics. Molecular Microbiology 80:612-627.

Figure Legends

Figure 1. Asymmetric polar gradients of cell envelope metabolic labeling in mycobacteria. A, Bacteria were incubated for 15 min in indicated probe or ~10% generation, then washed and fixed. The presence of alkynyl probes was detected by CuAAC with azido-488 and cells were imaged by structured illumination microscopy. B, *M. smegmatis* dual labeled with RADA and alkDADA, left, or RADA and OalkTMM, right. Bacteria were labeled and imaged as in A. C, *M. smegmatis* labeled as in A were imaged by conventional fluorescence microscopy and cellular fluorescence was quantitated for cells without (top; 77<n<85) or with (bottom; 9<n<51) visible septa for RADA (red), OalkTMM (light green) and alkDADA (dark green). Signal was normalized to cell length and to total fluorescence intensity. Cells were oriented such that the brighter pole is on the right hand side of the graph. D, *M. smegmatis* (dark blue) and *M. tuberculosis* (light blue) were labeled with HADA for 15 min and 2 hours, respectively, then

washed and fixed. Fluorescence was quantitated as in C for cells without (top; 34<n<42) and with (bottom; 9<n<31) visible septa. We defined the dim pole (dp; dark blue) as the sum of the fluorescence intensity over the first 25% of the cell; the sidewall (sw; medium blue) as the sum from 25% to 75%; and the bright pole (bp; light blue) as the sum over the final 25% of the cell. Fluor distrib, fluorescence distribution.

Figure 2. Multiple pathways of D-amino acid probe incorporation in *M. smegmatis.* A, Schematic of the theoretical routes of D-amino acid (DA) and D-alanine D-alanine (DADA) probe incorporation pathways. LDT, L,D-transeptidase, DDT, D,D-transpeptidase (DDTs). B, Sensitivity of HADA (blue), NADA (green), RADA (red), alkDA (white), alkDADA (grey) and OalkTMM (black) to antibiotics. *M. smegmatis* was pretreated or not with the indicated antibiotics at 2X MIC for 30 min then incubated an additional 15 min in the presence of probe. Then, the bacteria were washed and fixed. The alkyne-bearing probes were detected by CuAAC using the azido-carboxyrhodamine 110 label and quantitated by flow cytometry. Data are expressed as percentage of untreated wildtype labeling. Experiment was performed 3-4 times in triplicate and combined data are shown here. Error bars, +/- standard deviation. C, Additivity of HADA labeling inhibition by antibiotics. Imi, imipenem + clavulanate, amp, ampicillin + clavulanate, dcs, D-cycloserine. *M. smegmatis was* incubated in indicated combination of antibiotics and labeled as in B. Data are expressed as percentage of untreated labeling. The experiment was performed 3 times in triplicate and combined data are shown here. Error bars, +/- standard deviation. Additivity was assessed by comparing the effect of multiple antibiotics to treatment with the antibiotics individually. We show the higher p value of the two Student's unpaired two-sided t tests. *, $p < 0.05$, **, $p < 0.005$. D, Dose-dependent effect of imipenem on alkDADA (grey), HADA (blue) and RADA (red) labeling. *M. smegmatis* was pretreated or not with imipenem at the fold-MIC indicated and labeled as in B. Data are expressed as percentage of untreated labeling. The experiments were performed 3 times in triplicate and representative

data are shown here. Error bars, +/- standard deviation. E, Wildtype *M. smegmatis* pre-treated or not with 2X MIC imipenem and untreated *ΔldtABE* and the *ΔldtABE* + *ldtA* complement were labeled with alkDA (white), HADA (blue), NADA (green) or RADA (red) as in B. Experiment was performed 2-10 times (depending on the probe) in triplicate. Representative data from one of the biological replicates is shown here. Error bars, +/- standard deviation. MFI, median fluorescence intensity.

Figure 3. alkDADA rescues the growth of d-alanine racemase (Alr) and ligase (DdlA) mutants. alkDADA probe supports the growth of *Δalr*, A, or temperature-sensitive *ddlA*^{ts}, B. Wildtype (white bars) and *Δalr* (grey bars), B, or *ddlA*^{ts} (grey bars), were grown in the presence or absence of exogenous D-alanine, D-alanine-D-alanine or alkynyl derivatives thereof. Error bars, +/- standard deviation. Significant differences compared to *Δalr* no D-alanine (#, second bar from left), A, or *ddlA*^{ts} at 42 ˚C no D-alanine- D-alanine (#, fourth bar from left), B, Student's unpaired two-sided t test, are shown as *, $p < 0.05$, **, $p < 0.005$, ***, $p < 0.0005$, ****, $p<0.00005$. Data are combined from three independent experiments of 1-3 technical replicates each.

Figure 4. alkDADA and azDADA incorporate into lipid-linked peptidoglycan precursors. A, Detection of endogenous lipid-linked peptidoglycan precursors from organic extracts of *M. smegmatis*. Endogenous D-alanine were exchanged for biotin-D-lysine (BDL) via purified *S. aureus* PBP4 *in vitro*. Biotinylated species detected by blotting with streptavidin-HRP. MurJ (MviN) depletion strain was incubated in anhydrotetracycline (atc) to induce protein degradation. Other strains were treated with vancomycin (vanc), D-cycloserine (dcs) or a combination prior to harvesting. Wt, wildtype; blank, no sample run; no extract, BDL and PBP4 alone [a], organic extract from murJ-atc; [b], organic extract from murJ+atc; hk, heat-killed. B, Detection of lipid-linked peptidoglycan precursors that were labeled by alkDADA *in vivo*. Wildtype and *Δalr* strains

were incubated in alkDADA and treated or not with the indicated antibiotics prior to harvest. Alkyne-tagged species from organic extracts were ligated to picolyl azide biotin via CuAAC then detected as in A. BDL/PBP4, endogenous precursors from MurJ+atc were subjected to *in vitro* exchange reaction as in A. C, Detection of lipid-linked peptidoglycan precursors that were labeled by azDADA *in vivo*. *Δalr was* incubated in azDADA. Azide-tagged species from organic extracts were ligated to DIFO-biotin via SPAAC or to alkyne biotin via CuAAC then detected as in A.

Figure 5. alkDADA labeling is sensitive to periplasmic remodeling enzymes but can be stabilized by β-lactam treatment. A, Loss of LdtA, LdtB and/or LdtE decrease both RADA (red) and alkDADA (grey) labeling. Wildtype, *ldt* deletion mutants and the complemented strains were labeling for 30 min in triplicate. Bacteria were washed and fixed. alkDADA was detected by CuAAC using the azido-carboxyrhodamine 110 label. Fluorescence was quantitated by flow cytometry. Data are expressed as percentage of untreated wildtype labeling. Experiment was performed 7 times in triplicate and combined data are shown here. Error bars, +/- standard deviation. B, Additivity of RADA labeling in wildtype and *ΔldtABE*. Imi, imipenem + clavulanate, amp, ampicillin + clavulanate, dcs, D-cycloserine. *M. smegmatis* was pre-incubated in 2X MIC of indicated combination of antibiotics for 30 min then labeled with RADA for 15 min. Data for each strain are expressed as percentage of untreated labeling. Experiment was performed twice in triplicate and representative data are shown here. Error bars, +/- standard deviation. C, Imipenem or ampicillin rescues alkDADA labeling defect in *ΔldtABE*. Wildtype and *ΔldtABE M. smegmatis* were pretreated or not with 2X MIC of indicated antibiotics for 30 min then labeled with alkDADA for 15 min and processed as in A. MFI, median fluorescence intensity. Error bars, +/- standard deviation. D, Representative images and quantitation of cellular fluorescence for wildtype *M. smegmatis* +/- imipenem. 86<n<91. Signal was normalized by cell length and brighter poles oriented to the right-hand side of the graph. Arrows highlight sidewall signal.

Table S1: Strains used in this study.

Strain Name	Reference
M. smegmatis mc^{2}155	NC_008596 in GenBank
M. smegmatis MurJ (MviN) depletion strain	Gee CL, Papavinasasundaram KG, Blair SR, Baer CE, Falick AM, King DS, Griffin JE, Venghatakrishnan H, Zukauskas A, Wei JR, Dhiman RK, Crick DC, Rubin EJ, Sassetti CM, Alber T. Sci Signal. 2012 Jan 24;5(208):ra7.
M. smegmatis Δ*alr*	This study
M. smegmatis Δ*ldtA* (MSMEG_3528), Δ*ldtB* (MSMEG_4745), Δ*ldtE* (MSMEG_0233), and combinations	Provided by Dr. Kasia Baranowski and Dr. Eric Rubin; described in separate manuscript.
M. smegmatis ddlA^{ts}	Belanger AE, Porter JC, Hatfull GF. 2000. J. Bacteriol 182:6854-6856.
M. smegmatis pTetOldtA	Provided by Dr. Kasia Baranowski and Dr. Eric Rubin; described in separate manuscript.
M. tuberculosis mc^{2}6030 Δ*RD1* Δ*panCD*	Sambandamurthy VK, Derrick SC, Hsu T, Chen B, Larsen MH, Jalapathy KV, Chen M, Kim J, Porcelli SA, Chan J, Morris SL, Jacobs WR, Jr. 2006. Vaccine 24:6309-6320.

Supplemental Figure Legends

Figure S1. Penicillin-binding proteins are present along mycobacterial cell periphery. A, *M. smegmatis* merodiploid expressing PonA1-mRFP imaged by structured illumination microscopy. Longer arrow, polar and subpolar labeling. Short arrow, sidewall labeling. B, Bocillin labeling of live *M. smegmatis* pre-treated or not with ampicillin and clavulanate or D-cycloserine. No Boc, autofluorescence; no abx, no antibiotic pre-treatment. C, Quantitation of cellular fluorescence for B. 60<n<180. Signal was normalized by cell length and brighter poles oriented to the right-hand side of the graph.

Figure S2. Fluorescent vancomycin (vanc-fl) labeling at cell poles and in sidewall patches. *M. smegmatis* were incubated in the fluorescent antibiotic for 3 hrs or ~one doubling. Longer arrow, polar labeling. Short arrow, sidewall labeling.

Figure S3. Structures of D-amino acid probes. alkDA is detected by copper-catalyzed azide-alkyne cycloaddition (CuAAC) and HADA, NADA and RADA are one-step probes attached directly to fluorophores.

Figure S4. Metabolic labeling by azDADA comprises polar gradients in live *M. smegmatis*. Bacteria were labeled with azDADA for 15 min or ~10% generation and azDADA incorporation was detected by either A, low copper CuAAC (with BTTP ligand), or B, SPAAC. Longer arrow, polar labeling. Short arrow, sidewall labeling.

Figure S5. Heterogeneous envelope probe labeling in *M. tuberculosis.* A, *M. tuberculosis* was incubated for 2 hrs in NADA (green), HADA (blue) or RADA (red), washed and fixed. Fluorescence was assessed by flow cytometry. Note the cyan autofluorescence in middle panel.

B, *M. tuberculosis* was labeled with an amine-reactive dye (NHS488, black) then incubated or not for 2 hrs with HADA (dark blue), alkDA, alkDADA or OalkTMM. Alkynyl probes (light blue) and no probe control cells (grey) were detected by CuAAC with azido-coumarin. NHS488 labeling is heterogeneous and results in two distinct populations. While HADA labels both NHS488-positive and -negative bacteria, the two-step envelope probes preferentially incorporate into NHS488-positive *M. tuberculosis.* C, Fluorescence microscopy of HADA, alkDADA and OalkTMM-labeled bacteria in B. Envelope labeling is apparent both along the sidewall, where it colocalizes with NHS488, as well as at the cell poles, where it does not.

Figure S6. Physical expansion of the mycobacterial cell is confined to the poles. *M. smegmatis* were incubated in RADA for 45 min, washed then incubated briefly with NHS488, washed again and grown in the absence of probes for up to 45 min. Time lapse images were taken on an inverted Nikon TI-E microscope equipped with an environmental chamber that was maintained at 37 °C. Bacteria were imaged every 15 min in a microfluidic plate continuously perfused with growth medium. RADA (red) and NHS488 (green) fluorescence from a representative cell is quantified as in Fig. 2C and 2D.

Figure S7. Loss of LdtA, LdtB and LdtE do not cause a growth defect in *M. smegmatis.* Culture turbidity increases at the same rate for wildtype and *ΔldtABE* growing in 7H9 medium.

Figure S8. Imipenem increases fluorescent vancomycin (vanc-fl) labeling. *M. smegmatis* were incubated for 1 min with NHS-488 or grown in the presence of vanc-fl for 45 min then washed, fixed and analyzed by flow cytometry. MFI, median fluorescence intensity. Error bars, +/- standard deviation. Experiment was performed twice and representative data are shown.

Figure S9. alkDA labels at much lower concentrations than alkDADA. *M. smegmatis* were labeled with 2 mM of alkDADA (grey) or different concentrations of alkDA (white) for 15 min then fixed and subjected to CuAAC. MFI, median fluorescence intensity. Error bars, +/- standard deviation.

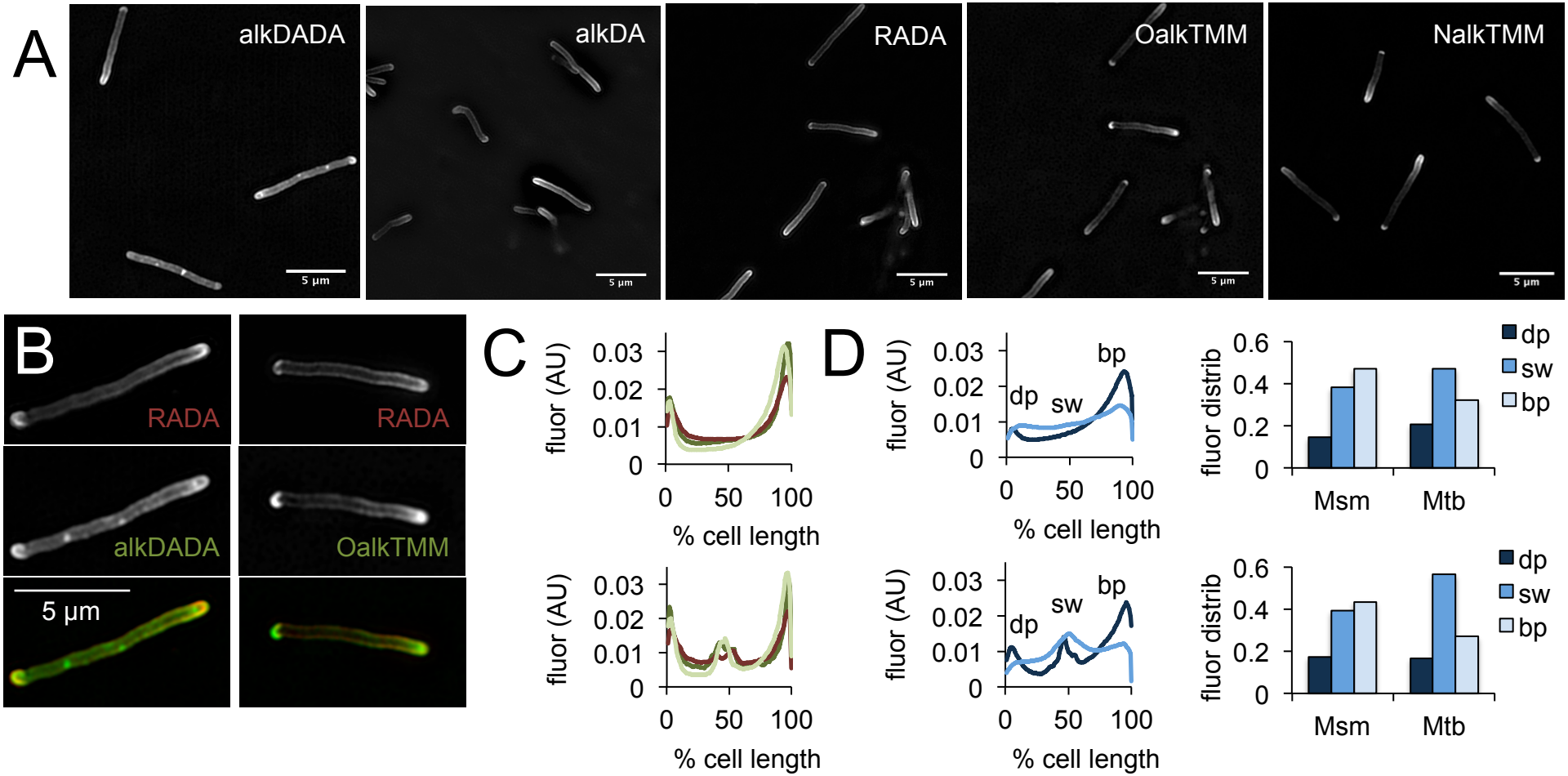

Figure 1. Asymmetric polar gradients of cell envelope metabolic labeling in mycobacteria. A, Bacteria were incubated for 15 min in indicated probe or ~10% generation, then washed and fixed. The presence of alkynyl probes was detected by CuAAC with azido-488 and cells were imaged by structured illumination microscopy. B, *M. smegmatis* dual labeled with RADA and alkDADA, left, or RADA and OalkTMM, right. Bacteria were labeled and imaged as in A. C, *M. smegmatis* labeled as in A were imaged by conventional fluorescence microscopy and cellular fluorescence was quantitated for cells without (top; 77<n<85) or with (bottom; 9<n<51) visible septa for RADA (red), OalkTMM (light green) and alkDADA (dark green). Signal was normalized to cell length and to total fluorescence intensity. Cells were oriented such that the brighter pole is on the right hand side of the graph. D, *M. smegmatis* (dark blue) and *M. tuberculosis* (light blue) were labeled with HADA for 15 min and 2 hours, respectively, then washed and fixed. Fluorescence was quantitated as in C for cells without (top; 34<n<42) and with (bottom; 9<n<31) visible septa. We defined the dim pole (dp; dark blue) as the sum of the fluorescence intensity over the first 25% of the cell; the sidewall (sw; medium blue) as the sum from 25% to 75%; and the bright pole (bp; light blue) as the sum over the final 25% of the cell. Fluor distrib, fluorescence distribution.

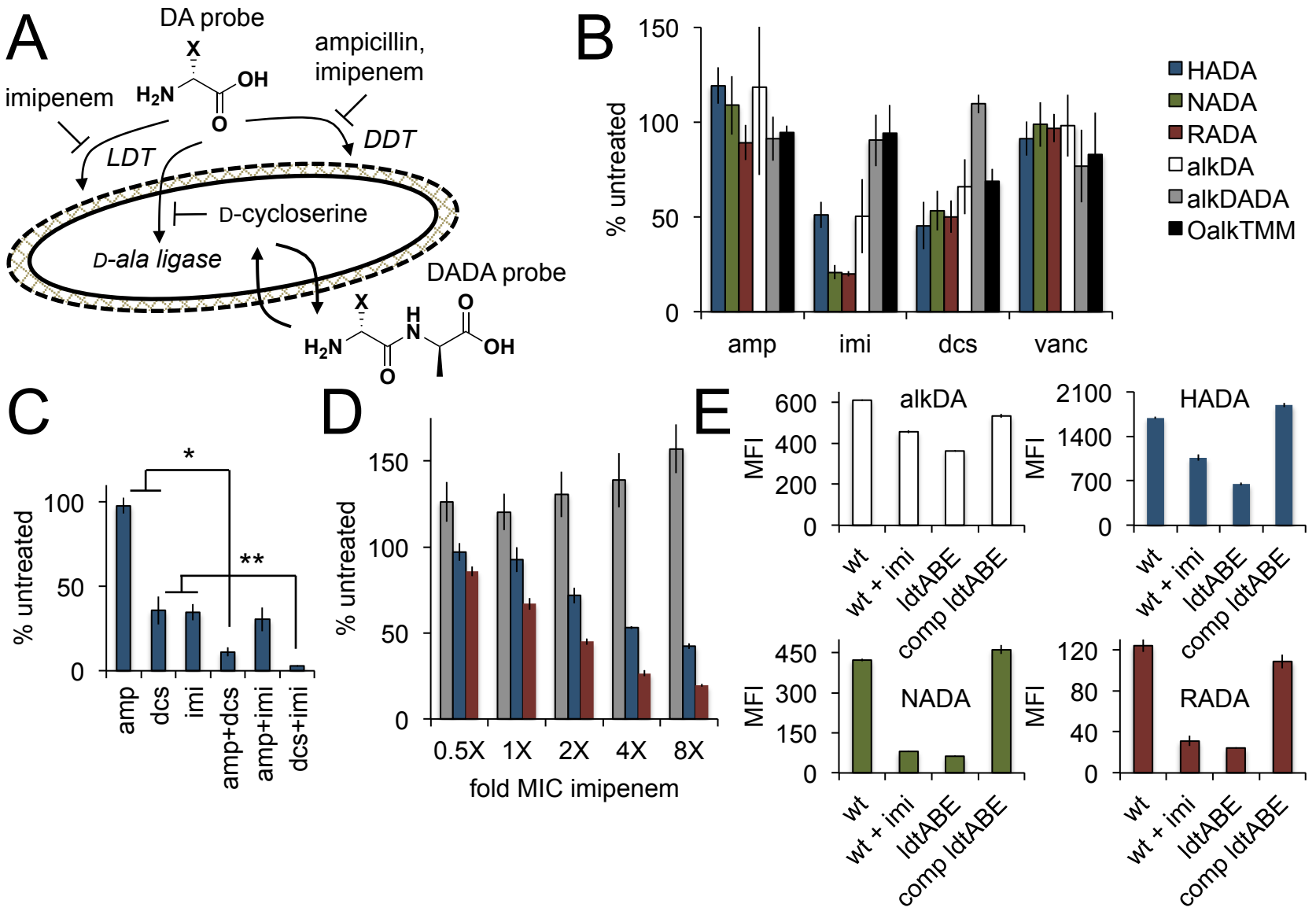
A
DA probe
X
H2N
OH
O
imipenem
ampicillin,
imipenem
LDT
DDT
D-cycloserine
D-ala ligase
DADA probe
X
H
N
O
H2N
OH
O
B
150
100
50
0
% untreated
amp
imi
dcs
vanc
HADA
NADA
RADA
alkDA
alkDADA
OalkTMM
C
*
**
100
50
0
% untreated
amp
dcs
imi
amp+dcs
amp+imi
dcs+imi
D
150
100
50
0
% untreated
0.5X
1X
2X
4X
8X
fold MIC imipenem
E
alkDA
600
400
200
0
MFI
HADA
2100
1400
700
0
MFI
NADA
450
300
150
0
MFI
RADA
120
80
40
0
MFI
wt
wt + imi
ldtABE
comp ldtABE

Figure 2. Multiple pathways of D-amino acid probe incorporation in *M. smegmatis.* A, Schematic of the theoretical routes of D-amino acid (DA) and D-alanine D-alanine (DADA) probe incorporation pathways. LDT, L,D-transeptidase, DDT, D,D-transpeptidase (DDTs). B, Sensitivity of HADA (blue), NADA (green), RADA (red), alkDA (white), alkDADA (grey) and OalkTMM (black) to antibiotics. *M. smegmatis* was pretreated or not with the indicated antibiotics at 2X MIC for 30 min then incubated an additional 15 min in the presence of probe. Then, the bacteria were washed and fixed. The alkyne-bearing probes were detected by CuAAC using the azido-carboxyrhodamine 110 label and quantitated by flow cytometry. Data are expressed as percentage of untreated wildtype labeling. Experiment was performed 3-4 times in triplicate and combined data are shown here. Error bars, +/- standard deviation. C, Additivity of HADA labeling inhibition by antibiotics. Imi, imipenem + clavulanate, amp, ampicillin + clavulanate, dcs, D-cycloserine. *M. smegmatis was* incubated in indicated combination of antibiotics and labeled as in B. Data are expressed as percentage of untreated labeling. The experiment was performed 3 times in triplicate and combined data are shown here. Error bars, +/- standard deviation. Additivity was assessed by comparing the effect of multiple antibiotics to treatment with the antibiotics individually. We show the higher p value of the two Student's unpaired two-sided t tests. *, $p < 0.05$, **, $p < 0.005$. D, Dose-dependent effect of imipenem on alkDADA (grey), HADA (blue) and RADA (red) labeling. *M. smegmatis* was pretreated or not with imipenem at the fold-MIC indicated and labeled as in B. Data are expressed as percentage of untreated labeling. The experiments were performed 3 times in triplicate and representative data are shown here. Error bars, +/- standard deviation. E, Wildtype *M. smegmatis* pre-treated or not with 2X MIC imipenem and untreated *ΔldtABE* and the *ΔldtABE* + *ldtA* complement were labeled with alkDA (white), HADA (blue), NADA (green) or RADA (red) as in B. Experiment was performed 2-10 times (depending on the probe) in triplicate. Representative data from one of the biological replicates is shown here. Error bars, +/- standard deviation. MFI, median fluorescence intensity.

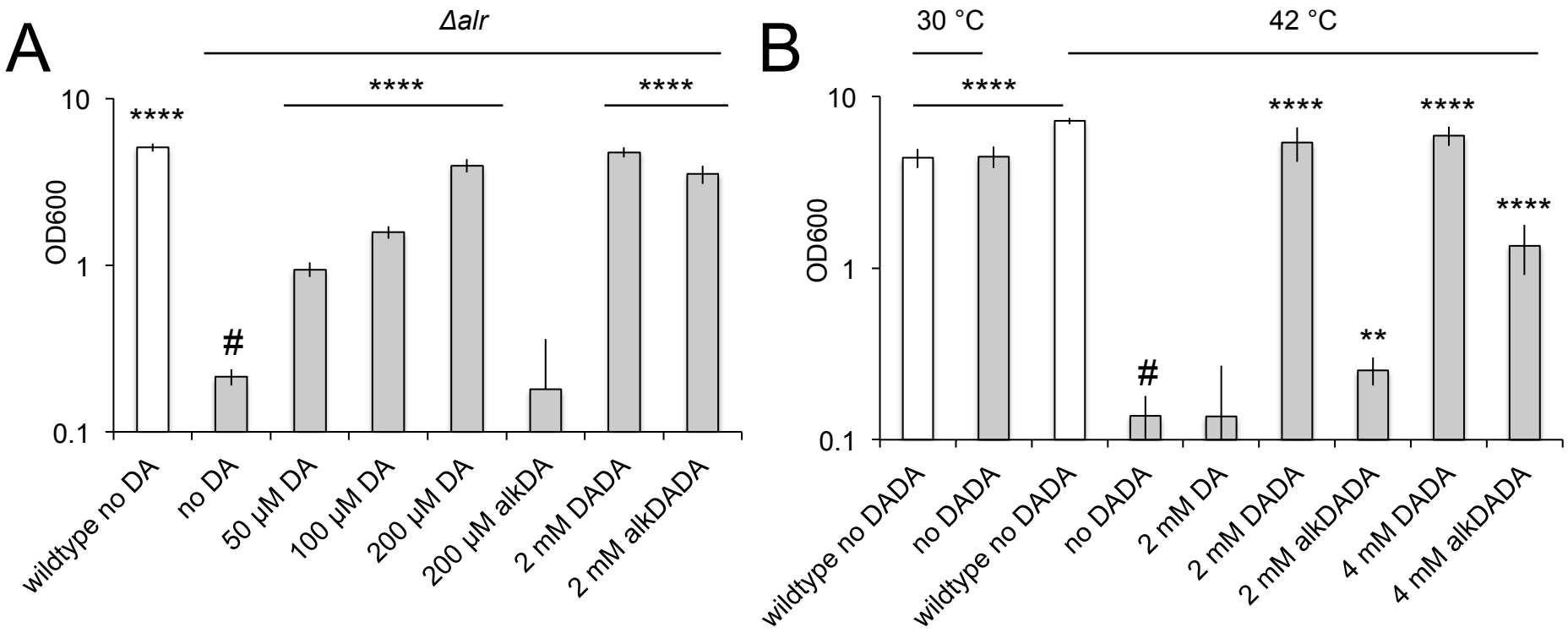

Figure 3. alkDADA rescues the growth of D-alanine racemase (Alr) and ligase (DdlA) mutants. alkDADA probe supports the growth of *Δalr*, A, or temperature-sensitive *ddlA*^{ts}, B. Wildtype (white bars) and *Δalr* (grey bars), B, or *ddlA*^{ts} (grey bars), were grown in the presence or absence of exogenous D-alanine, D-alanine-D-alanine or alkynyl derivatives thereof. Error bars, +/- standard deviation. Significant differences compared to *Δalr* no D-alanine (#, second bar from left), A, or *ddlA*^{ts} at 42 ˚C no D-alanine-D-alanine (#, fourth bar from left), B, Student's unpaired two-sided t test, are shown as *, $p < 0.05$, **, $p < 0.005$, ***, $p < 0.0005$, ****, $p<0.00005$. Data are combined from three independent experiments of 1-3 technical replicates each.

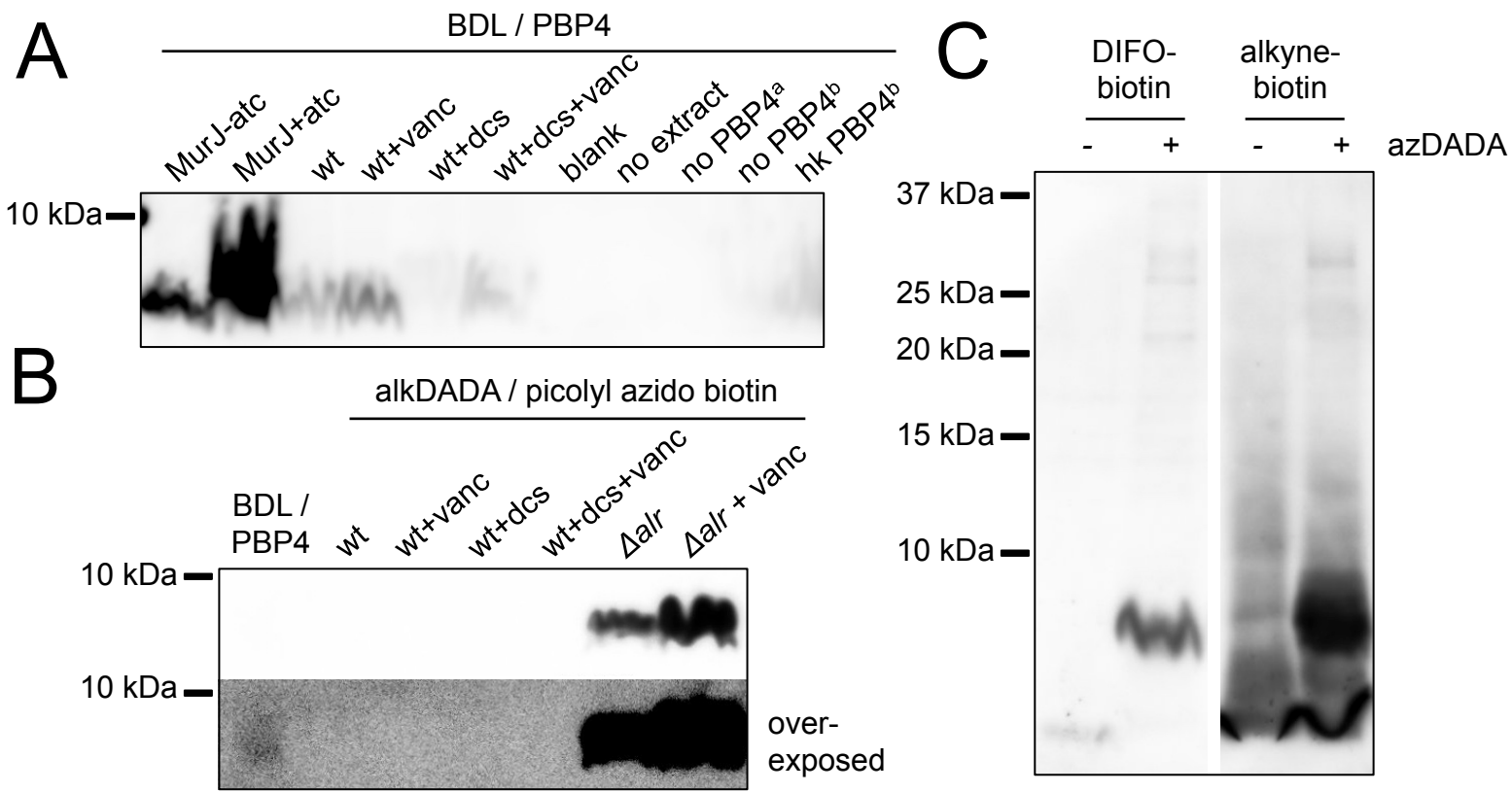

Figure 4. alkDADA and azDADA incorporate into lipid-linked peptidoglycan precursors. A, Detection of endogenous lipid-linked peptidoglycan precursors from organic extracts of *M. smegmatis*. Endogenous D-alanine were exchanged for biotin-D-lysine (BDL) via purified *S. aureus* PBP4 *in vitro*. Biotinylated species detected by blotting with streptavidin-HRP. MurJ (MviN) depletion strain was incubated in anhydrotetracycline (atc) to induce protein degradation. Other strains were treated with vancomycin (vanc), D-cycloserine (dcs) or a combination prior to harvesting. Wt, wildtype; blank, no sample run; no extract, BDL and PBP4 alone [a], organic extract from murJ-atc; [b], organic extract from murJ+atc; hk, heat-killed. B, Detection of lipid-linked peptidoglycan precursors that were labeled by alkDADA *in vivo*. Wildtype and *Δalr* strains were incubated in alkDADA and treated or not with the indicated antibiotics prior to harvest. Alkyne-tagged species from organic extracts were ligated to picolyl azide biotin via CuAAC then detected as in A. BDL/PBP4, endogenous precursors from MurJ+atc were subjected to *in vitro* exchange reaction as in A. C, Detection of lipid-linked peptidoglycan precursors that were labeled by azDADA *in vivo*. *Δalr was* incubated in azDADA. Azide-tagged species from organic extracts were ligated to DIFO-biotin via SPAAC or to alkyne biotin via CuAAC then detected as in A.

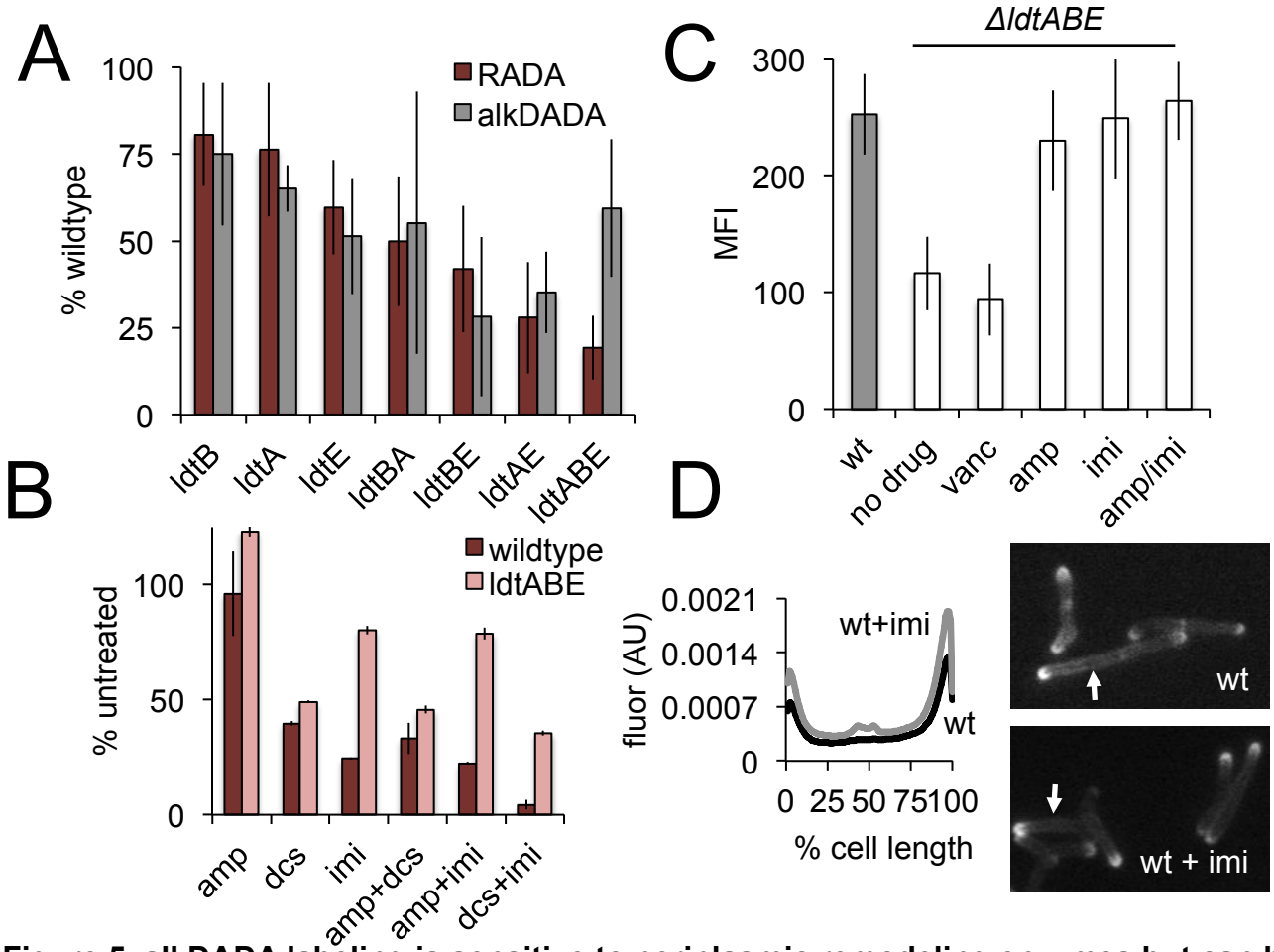

Figure 5. alkDADA labeling is sensitive to periplasmic remodeling enzymes but can be stabilized by β-lactam treatment. A, Loss of LdtA, LdtB and/or LdtE decrease both RADA (red) and alkDADA (grey) labeling. Wildtype, *ldt* deletion mutants and the complemented strains were labeling for 30 min in triplicate. Bacteria were washed and fixed. alkDADA was detected by CuAAC using the azido-carboxyrhodamine 110 label. Fluorescence was quantitated by flow cytometry. Data are expressed as percentage of untreated wildtype labeling. Experiment was performed 7 times in triplicate and combined data are shown here. Error bars, +/- standard deviation. B, Additivity of RADA labeling in wildtype and *ΔldtABE*. Imi, imipenem + clavulanate, amp, ampicillin + clavulanate, dcs, D-cycloserine. *M. smegmatis* was pre-incubated in 2X MIC of indicated combination of antibiotics for 30 min then labeled with RADA for 15 min. Data for each strain are expressed as percentage of untreated labeling. Experiment was performed twice in triplicate and representative data are shown here. Error bars, +/- standard deviation. C, Imipenem or ampicillin rescues alkDADA labeling defect in *ΔldtABE*. Wildtype and *ΔldtABE M. smegmatis* were pretreated or not with 2X MIC of indicated antibiotics for 30 min then labeled with alkDADA for 15 min and processed as in A. MFI, median fluorescence intensity. Error bars, +/- standard deviation. D, Representative images and quantitation of cellular fluorescence for wildtype *M. smegmatis* +/- imipenem. 86<n<91. Signal was normalized by cell length and brighter poles oriented to the right-hand side of the graph. Arrows highlight sidewall signal.